

FACULTY OF SCIENCE
UNIVERSITY OF COPENHAGEN

Master Thesis

Martin Kufahl



Experimental Methods

for Implementing Electron Spin Qubits
in Double Quantum Dots

June 16, 2014

Supervisor: Prof. Charles Marcus

Center for
Quantum
Devices



Abstract

To achieve universal quantum computation it is necessary to encode quantum information in a physical system, called a quantum bit or *qubit*. These can be realized in a multitude of ways, and the aim of this Master's project has been to explore one possibility in which the spin states of entangled electrons encode quantum information, known as *electron spin qubits*. The thesis contains a description of the experimental setup and techniques used to confine electrons in lateral, gate-defined double quantum dot (DQD) systems for potential use as electron spin qubits, as well as experimental control routines used and/or developed during the project. Experimental results are presented to elucidate the possibilities and limitations of the measured devices for use as DQD systems, as well as quantifying the performance of the reflectometry circuit used for fast readout of charge sensing. The main focus of the thesis has been to provide new experimentalists with an overview of the experimental setups and techniques used for electron spin qubit experiments at Center for Quantum Devices.

Contents

| | |
|--|------------|
| List of Figures | iii |
| 1 Introduction | 1 |
| 2 Electron spin qubits | 3 |
| 2.1 Quantum information processing | 3 |
| 2.1.1 Physical implementations of qubits | 4 |
| 2.1.2 Lateral gate-defined quantum dots | 5 |
| 2.1.3 Double quantum dots | 6 |
| 3 Experimental setup | 8 |
| 3.1 Overview | 8 |
| 3.2 Devices | 9 |
| 3.2.1 CB7 devices | 12 |
| 3.2.2 NO7 devices | 13 |
| 3.3 Sample board | 15 |
| 3.4 Cryostat | 18 |
| 3.4.1 Cryostat layout | 19 |
| 3.4.2 The Pulse Tube Refrigerator | 20 |
| 3.4.3 The Dilution Unit | 20 |
| 3.4.4 Sample loading | 21 |
| 3.5 Electronics | 22 |
| 3.5.1 DC lines | 22 |
| 3.5.2 RF lines | 27 |
| 3.5.3 Demodulation circuit | 29 |
| 3.5.4 Alazar digital oscilloscope | 31 |
| 3.6 Data acquisition | 33 |
| 3.6.1 Useful Igor functions | 34 |
| 4 Measurement techniques | 37 |
| 4.1 Cooldown tests | 38 |

| | | |
|----------|--|-----------|
| 4.1.1 | Bias cooling | 39 |
| 4.1.2 | Quantum point contacts | 40 |
| 4.1.3 | Quantum dots | 42 |
| 4.2 | Charge sensing | 43 |
| 4.3 | Reflectometry | 48 |
| 4.3.1 | Impedance matching | 49 |
| 4.3.2 | Demodulation | 50 |
| 4.3.3 | Fast readout | 53 |
| 5 | Igor routines | 55 |
| 5.1 | Charge sensor compensation | 55 |
| 5.1.1 | Calibration of SQD coupling strengths | 57 |
| 5.2 | Automatic charge sensor calibration | 60 |
| 5.3 | Automatic backup of DAC state of scans | 61 |
| 5.4 | FeatureScan() | 63 |
| 6 | Results | 66 |
| 6.1 | Pauli spin blockade in NO7a DQD | 69 |
| 6.2 | Fast readout via reflectometry | 70 |
| 6.3 | Asymmetric double quantum dots | 72 |
| 7 | Summary and outlook | 74 |
| A | Error signature of faulty DC block | 76 |
| | Epilogue | 77 |
| | Bibliography | 81 |

List of Figures

| | | |
|------|--|----|
| 3.1 | Schematic of a GaAs heterostructure used for sample fabrication . . . | 10 |
| 3.2 | SEM image of a CB7 device. | 12 |
| 3.3 | Design file of NO7 device | 13 |
| 3.4 | SEM image of NO7a | 14 |
| 3.5 | Mayo Board V1R1 | 15 |
| 3.6 | CB7 sample bonded onto Mayo V1R1 sample board. | 17 |
| 3.7 | Sample bonded to Mayo board, mounted in 51-14 puck. | 18 |
| 3.8 | Triton 200 helium dilution refrigerator | 19 |
| 3.9 | Sample puck loaded onto cryostat cold finger | 21 |
| 3.10 | Electronic circuit of the experimental setup | 23 |
| 3.11 | Picture of the electronics used in the experimental setup | 26 |
| 3.12 | Diagram of the demodulation circuit used in reflectometry. | 29 |
| 4.1 | Schematic illustration of a quantum point contact (QPC) | 40 |
| 4.2 | Conductance of QPC channel in CB7 device versus gate voltage . . . | 41 |
| 4.3 | Wall/wall scan of quantum dot in NO7a | 42 |
| 4.4 | Coulomb peaks in S2 sensor quantum dot in NO7a | 43 |
| 4.5 | Charge sensing using QPC in CB7 device | 44 |
| 4.6 | NO7a configured for charge sensing of a DQD via a sensor quantum dot | 45 |
| 4.7 | Charge sensing measurement versus transport measurement in DQD | 46 |
| 4.8 | Charge sensing using conductance measured via SR830 Lock-in amplifier | 47 |
| 4.9 | Impedance matching in CB7 3_4 | 50 |
| 4.10 | Circuit diagram of a double-balanced frequency mixer | 51 |
| 4.11 | Charge sensing using conductance measured via reflectometry circuit | 52 |
| 4.12 | Charge sensing of NO7a triple-dot "house" structure with transport and reflectometry | 52 |
| 4.13 | Fast readout of charge sensing via reflectometry | 54 |
| 4.14 | Fast reflectometry readout sweeps concatenated | 54 |

| | | |
|-----|---|----|
| 5.1 | Compensated charge sensing of double quantum dot | 59 |
| 5.2 | Demonstration of FeatureScan() function showing bias triangles at various wall voltages | 65 |
| 6.1 | SEM micrograph of blown device NO7b. | 67 |
| 6.2 | Charge sensing measurement of asymmetric DQD in NO7a with significant sensor noise. | 68 |
| 6.3 | Pauli spin blockade demonstrated in Q11/Q12 DQD in device NO7a | 69 |
| 6.4 | Charge sensing of a triple point in a DQD | 70 |
| 6.5 | Raw demodulated reflectometry signal acquired by Alazar | 70 |
| 6.6 | Autocorrelation of raw reflectometry signal | 71 |
| 6.7 | Fourier transform of raw reflectometry signals | 72 |
| 6.8 | Fast charge sensing of bias triangle of asymmetric DQD in NO7a . . | 73 |
| A.1 | S_{21} reflection of reflectometry lines in cryostat with faulty DC block, measured with a network analyzer | 76 |

1

Introduction

*Plunge your army into desperate straits and it will come off in safety;
place it in deadly peril and it will survive.*^[27]

In this thesis I introduce the concept of electron spin qubits, as well as their implementation in lateral, gate-defined double quantum dots (DQDs) in a GaAs / AlGaAs heterostructure.

The primary focus of the thesis is on the practical aspect of conducting experiments on quantum devices using a cryostat and relevant electronics. I have endeavoured to craft a document that, aside from describing the Master's project I have undertaken, might also serve as a general introduction to the devices, instruments and methods currently used for creating and measuring lateral quantum dot structures, which have potential applications for quantum information processing. If I have succeeded, perhaps this document will prove useful for the next generations of eager students joining the Center for Quantum Devices.

The original aim of the project was to investigate the potential of variants of the double quantum dot (DQD) system for use in implementing *singlet-triplet* (S-T₀) qubits, originally proposed in 2002 by J. Levy. A qubit is a quantum two-level system which can be used to encode quantum information, for potential use in quantum computing. In an S-T₀ qubit, the two levels are spin states of a pair of entangled electrons, in the subset of spin states with total angular momentum $m = 0$, known as a *decoherence-free subspace*^[15].

The system was implemented in by J. Petta *et al.* in 2005^[19], who demonstrated the confinement and entanglement of two electrons in a DQD, as well as initialization, coherent manipulation and measurement of the two-electron spin qubit. The

measurements were made on ensembles of identically prepared and manipulated systems, but later developments by Barthel *et al.*^[1, 2] demonstrated *single-shot read-out* using high-frequency sensing techniques described in chapter 4 in this thesis, in which the state of a single qubit can be read out with >90% fidelity.

So far, the singlet-triplet qubits described have consisted of only two electrons. However, it was shown by Higginbotham *et al.*^[12] that operating the same device in the multi-electron regime had beneficial effects on the coherence time of the qubit, although this was for a particular device and electron occupation. There is also the possibility of asymmetric double quantum dot systems, in which the two quantum dots were not identical in dimensions. This thesis project was intended as an expedition into this as yet uncharted territory.

Some headway was made, although we did not reach the point of demonstrating full initialization and measurement of spin qubits. As is often the case in experimental physics, the road is fraught with technical challenges that must be overcome. While I did not reach the original goal of the expedition, I have become well acquainted with many practical techniques involved in cooling and measuring on quantum dot devices, and have tried to condense the accumulated knowledge and experience into this document.

I have included a brief introduction to the theory behind quantum dots confined in a 2-dimensional electron gas. For a more thorough description of the physical parameters of the system I refer to the excellent Ph.D. thesis "Charge Sensing and Spin Dynamics in GaAs Quantum Dots" by Alexander Johnson, as well as the high-information density review from 2007 by Hanson *et al.*^[11]

"But this isn't war!"

- Martin

"You're right. It's science, it's supposed to be fun!"

- Charlie

2

Electron spin qubits

This section will briefly introduce the principle of using spins of entangled electrons to encode quantum information, ie. a physical implementation of a qubit.

2.1 Quantum information processing

Perhaps the most notable technological advance of the 20th century has been the invention of computers, which has influenced our society in ways too profound to imagine, at least without a few hundred years' worth of historical hindsight. At its core, what we now call *classical* computation is the processing of information using purely binary logic. The fundamental unit of information used is the *bit*, which is any system that can be in either one state or the other. On or off, zero or one.

Nature, however, does not feel Herself confined to such absolutes. A revolutionary feature introduced by quantum mechanics is that a system may very well be in a state of zero *and* one. Or to use the popular image of an unfortunate cat - alive *and* dead. It is only in the act of interacting with the surrounding universe that a system "decides" on a particular value.

Consider a system that can be in one of two states, subject to quantum mechanics. The spin of an electron, for example - up or down? When nobody is looking, probably a bit of both. The electron wavefunction is in some superposition of the two *basis states* used to denote the logical qubit:

$$|\psi\rangle = \alpha|0\rangle + \beta|1\rangle$$

and the superposition can be used to define another fundamental unit of information - a *qubit*. α and β are probability amplitudes, and when performing a measurement on the qubit the probability of measuring the $|0\rangle$ state is $|\alpha|^2$. Imagine, then, a computer which operates not with classical bits, but with quantum bits. It is a *quantum information processor*, subject to entirely different game rules than its classical counterpart, which opens new avenues of possibility but also comes with

a range of limitations.

In a classical computer, information is processed by subjecting the bits pairwise to a set of *logic gates*, such as AND, OR, NOT and so forth. Quantum information processing similarly boils down to subjecting the qubits to a set of logical gates with names such as the *Hadamard gate*, *Toffoli gate*, *controlled-not* or CNOT gate, etc., which operates on the wavefunctions of the qubits. A crucial difference between classical and quantum logical operations is that the latter are *reversible*, or in mathematical terms, the qubit operators are *unitary*.

For a given input, the classical computation will deterministically result in exactly one output. This is not the case in quantum computing, where the measurement of identically prepared systems yield probabilistic results determined by the probability amplitudes. The challenge of quantum information processing is then to manipulate the system such that the desired outcomes become most probable, and the same calculation can be performed until the total set of solutions can be obtained statistically. For a certain type of problems in computer science, such as the factorization of large numbers into prime numbers, quantum computation promises exponentially faster computation times, to the point where a calculation that might take the fastest classical computer a hundred years to complete might be achieved by a hypothetical, functioning quantum computer in a matter of hours^[6].

The profound possibilities of quantum information processing have amused mathematicians and computer scientists since the 80's, but implementing the abstract qubits and quantum logic gates in physical systems is a highly technically demanding challenge, and physicists today are still searching for stable and dependable systems for encoding and controlling quantum information.

2.1.1 Physical implementations of qubits

There is an apparent paradox in envisioning a qubit for quantum information processing. Quantum information is notoriously unstable - interaction with the environment will cause the wavefunction to collapse, at the loss of quantum information. It is said that the system *decoheres*. It is therefore necessary to isolate the qubit from the environment, and the *coherence time* is an important figure of merit for a potential qubit.

Conversely, a system that is highly decoupled from the environment tends to also couple weakly with other qubits, and measuring the qubit becomes challenging. A balance must be struck between the two extremes, and it is likely that a working quantum computer relies on different types of qubits for different functions, similar to how classical computers employ different types memory types for information processing and long-term storage.

Similar to the wide variety of ways the classical bit has been implemented, be

it in states of a transistor, magnetic polarizations on a harddisk, microscopic holes on a CD etc., there are many ways to physically implement a qubit. Any quantum two-level system will do, be it the spin of an electron, the polarization of a photon, or some exotic system such as a flux quantum of a superconductor. In experimental quantum physics today, each possibility has its own research field in pursuit of the most reliable and efficient qubit implementation. We find ourselves in the field of *solid state qubits*. The promise of this particular avenue of research is that semiconductor technology has already been developed considerably due to the ubiquity of classical computers.

2.1.2 Lateral gate-defined quantum dots

One notable achievement has been the confinement of single electrons in *quantum dots*. A quantum dot is a general term for a quantum system confined in all three physical dimensions. Quantum dots have been realized in a multitude of ways, but the ones exclusively concerned with in this thesis are *lateral gate-defined quantum dots*, in which individual electrons are trapped and can be used to encode quantum information. The method for confining quantum dots will be elaborated upon in section 3.2, but a brief introduction will be given here.

First and foremost, lateral quantum dots rely on a *two-dimensional electron gas* or *2DEG*, in which electrons are quantum confined in one dimension and thus confined to a plane. This is achieved by manufacturing a layered semiconductor heterostructure, in our case of the GaAs / AlGaAs type. The planar nature is what makes these quantum dots *lateral*. The second part, *gate-defined*, is due in the fact that electrodes called *gates* in the trade are deposited on the surface of the heterostructure, and applying a voltage to these gates changes the electrostatic potential of the electrons underneath. The gates can be designed with very high resolution, on the order of tens of nm. Through the gates, the experimentalist can selectively "deplete" the 2DEG underneath, and thus design the confinement potential of the electrons, subject to challenges in fabrication which are altogether not trivial. A great deal of effort by a group of people in *Center for Quantum Devices* is dedicated towards designing and fabricating devices that allows the formation of various systems of quantum dots, potentially with the ability of hosting scalable arrays of solid state qubits.

The quantum mechanics of a single quantum dot can be roughly estimated by the two-dimensional *particle in a box* approximation. An electron in a semiconductor behaves approximately like a free particle, albeit with a material-specific effective mass m^* . For GaAs, where the confined 2DEG "lives", $m^* = 0.067m_0$, where m_0 is the mass of a free electron.

The energy of the electron is then given by:

$$E = \frac{\hbar^2 \mathbf{k}^2}{2m^*} \quad (2.1)$$

where \mathbf{k} is the *wave vector*, which in the case of a two-dimensional system with lengths L_x and L_y , is given by:

$$\mathbf{k}_{\mathbf{n}_x, \mathbf{n}_y} = k_{n_x} \hat{\mathbf{x}} + k_{n_y} \hat{\mathbf{y}} = \frac{n_x \pi}{L_x} \hat{\mathbf{x}} + \frac{n_y \pi}{L_y} \hat{\mathbf{y}}. \quad (2.2)$$

where n_x, n_y are the quantum numbers corresponding to the standing wave solutions to the Schrödinger equation.

While the actual electronic potentials in lateral quantum dots are more akin to highly dynamic valley potentials, the above equation can provide a rough estimate of the dynamics. A quantum dot can hold a finite amount of electrons, separated in energy by the *level spacing* as well as the Coulomb interaction between the particles. In a 2DEG, states will be filled from electrons until the Fermi level E_F . By controlling the electrostatic potential via the gates, one can then selectively fill a number of electrons in a lateral quantum dot confined in the 2DEG.

2.1.3 Double quantum dots

If two quantum dots are formed in close proximity with some overlap of the electronic wavefunctions, a *double quantum dot* is formed. This system enables many interesting control dynamics, such as control of the relative energy levels in the dots, as well as the degree of interdot coupling, t_c . The *Loss-DiVincenzo* qubit proposed in 1997^[16] consists of a double quantum dot structure, where the spin of an electron in either dot encode the respective qubits. This system is prone to decoherence as the electrons are very strongly coupled to the environment through charge interactions, but there are other methods of encoding qubits in double quantum dot systems available. In particular, the *Singlet-Triplet* (or S-T₀) qubit was of interest for this Master's project, although a full implementation was not demonstrated. Regardless, the relevant theory will be briefly introduced.

If two electrons populate a single quantum dot, the energetically most favourable configuration is the *singlet* state, where both electrons occupy the ground state orbital with opposite spins ie. $|\uparrow\downarrow\rangle$. If a second quantum dot is introduced, coupled to the first dot by the tunnel coupling t_c and with an independently controlled electrostatic potential, the possibility of the electrons occupying one quantum dot each opens up. Let us call the two charge occupations (1,1) and (0,2), respectively. At a particular relative electric potential, the two charge states are degenerate. We introduce parameter of *detuning*, ϵ , which is the relative voltage difference from this

point. If $\epsilon < 0$, the (1,1) configuration is the ground state, and at $\epsilon > 0$, the (0,2) is the ground state.

In the case of large detuning towards (1,1) occupation, the two electrons are effectively separated from each other, and their spins can precess relative to each other without paying any penalty in energy due to Pauli exclusion. Thus, a double quantum dot system with (1,1) electron occupation can exist in four spin states; the *singlet* state:

$$|S\rangle = (|\uparrow\downarrow\rangle - |\downarrow\uparrow\rangle)/\sqrt{2}$$

with total spin $S = 0$, and three *triplet* states with total spin $S = 1$:

$$|T_+\rangle = (|\uparrow\uparrow\rangle$$

$$|T_0\rangle = (|\uparrow\downarrow\rangle + |\downarrow\uparrow\rangle)/\sqrt{2}$$

$$|T_-\rangle = (|\uparrow\uparrow\rangle$$

So called because the energy states are triplet degenerate, at least in the absence of magnetic field. In the *presence* of a such field B_z , the energy levels are separated as they have angular momentum in the axis of the magnetic field of m_z of +1, 0 and -1 respectively, due to *Zeeman splitting* with the Hamiltonian term:

$$H_Z = g\mu_B\hat{S} \quad (2.3)$$

where g is the g-factor of the host material, in GaAs $g \sim -0.4$; μ_B is the Bohr magneton and \hat{S} is the spin vector. The result is that the $|T_+\rangle$ and $|T_-\rangle$ states separate in energy by $E_Z = g\mu_B B_{\text{ext}}$, whereas the $m_z = 0$ states $|T_0\rangle$ and $|S\rangle$ remain unaffected.

These two states, $|T_0\rangle$ and $|S\rangle$, are thus practically degenerate for $\epsilon < 0$. Ignoring excited states, the system exists in a superposition of singlet and triplet and these states can suitably be used to denote the logical basis of a qubit - hence *singlet-triplet qubit*. For positive detuning, $\epsilon > 0$, the two states depart in energy, and changing the detuning thus corresponds to a projective measurement on the qubit. This also mean that the qubit can be *initialized* by adiabatically sweeping the detuning into the (0,2) regime, which will ensure that the qubit is in the energetically favoured singlet state.

3

Experimental setup

To create and control a physical implementation of a qubit, one must rely on a wide array of technologically highly refined methods and machinery. In this chapter I will describe the experimental setup, paying homage to my training in nanoscience by adopting a "bottom-up" approach, starting with the fabrication of the quantum devices, proceeding with the electrical integration of the device with the experimental setup, the cryostat used for achieving the necessary cryogenic temperatures, the electronic circuitry facilitating measurements of the system, and finally the hardware and software architecture that enables data acquisition and processing.

3.1 Overview

The devices measured were gated lateral quantum dot systems, fabricated on a GaAs / AlGaAs semiconductor heterostructure wafer. Fine metal electrodes ("gates") have been deposited on top of the semiconductor wafer with electron-beam lithography techniques, and voltages are applied to these which depletes the twodimensional electron gas, referred to as *2DEG*, situated at the GaAs / AlGaAs interface. This enables control of the electrical potential landscape, and quantum dots can be formed in the 2DEG. The electron gas itself is also contacted through "ohmic" contacts, and current through quantum dots can be measured.

The *sample* refers to a chip of semiconductor heterostructure with a device fabricated on it. Often, several individual devices are made on the same chip. The chip is glued onto a sample holder, in our case a Mayo PCB sample board as described in section 3.3. The sample holder provides the electrical interface between the device and the electrical wiring of the cryostat, and contains various circuit elements necessary for electrical measurement of the device. The sample board is electrically connected to the quantum device via thin aluminium wires, deposited with a wire

bonder. The Mayo board is mounted inside a brass cylinder ("slug"), which in turn can be mounted inside a cryostat to achieve cryogenic temperatures of the device.

The cryostats used in Center for Quantum Devices are closed-cycle, cryo-free helium dilution refrigerators, of the type Triton 200 made by Oxford Instruments, which are described in section 3.4. The cryostat can reach a base temperature of approximately 20 mK, which is sufficiently low to avoid thermal excitation of electrons to excited states¹. The cryostat provides electrical access to the sample slug through both DC lines and coax lines suitable for high-frequency applications, which play a crucial role in measurement and control of solid state qubits.

Outside of the cryostat, the experimentalist employs a wide variety of electronic instruments to conduct an experiment. Notable instruments include digital-to-analog converters ("DACs") which provide a voltage source for the individual gates and contacts of the device; current preamplifiers and digital multimeters ("DMMs") to allow measurement of a current eg. through a quantum dot; lock-in amplifiers for much the same purpose; various signal generators for supplying high-frequency RF signals, and oscilloscopes for measuring the electrical responses of the devices under test. The electronic setup is shown in figure 3.10 (page 23).

The instruments are connected to a data acquisition computer running a data analysis program, in our case Igor Pro, with functions customized for the instruments and experiment in question. This enables the experimentalist(s) to control the experiment, as well as collecting and analyzing data.

3.2 Devices

Several devices have been used during the experimental run, all designed for forming lateral quantum dots in a 2-dimensional electron gas (2DEG), used to trap individual electrons to act as carriers of quantum information via their spin ie. electron spin qubits. The 2DEGs are contained in semiconductor heterostructures, and the quantum dots are formed through selectively depleting areas of the 2DEG in all three spatial dimensions. The various aspects of electron spin qubit systems will be explained below.

The devices were fabricated by two different people on separate occasions; the "CB7" devices were made by Christian Barthel in 2006 during his Ph.D. programme at Harvard University, and the "NO7" devices were made by Nastasia Okulova in 2013 during her Master's programme at Center for Quantum Devices. The devices were fabricated on two different wafers of GaAs / AlGaAs heterostructures supplied externally by specialized growers.

¹ $E = k_{\text{B}}T = 8.62 \cdot 10^{-5} \frac{\text{eV}}{\text{K}} * 20\text{mK} \approx 1.7\mu\text{eV}$

The heterostructures were grown on GaAs substrates using molecular beam epitaxy (MBE). First, to eliminate lattice defects from the GaAs substrate, alternating layers of GaAs and $\text{Al}_x\text{Ga}_{1-x}\text{As}$ (typically $\text{Al}_{0.3}\text{Ga}_{0.7}\text{As}$, referred to here simply as AlGaAs) are deposited. A layer of GaAs is then deposited on the wafer, typically hundreds of nm deep. The next section deposited consists of AlGaAs, some tens of nm deep. A single layer of Si dopant atoms are then deposited ("delta-doping"), the distance to the interface and density of dopant atoms being significant parameters for the properties of the wafer. Deposition of AlGaAs is then resumed until a chosen height is reached. Finally, a thin (~ 10 nm) layer of GaAs is deposited to protect the AlGaAs layer underneath. Refer to figure 3.1a for the wafer used to fabricate the CB7 devices.

The Si doping introduces free electrons into the semiconductor crystal, which will form the 2-dimensional electron gas. To understand how the electrons are confined in the heterostructure, it is useful to review the basics of band structure theory in solid state physics. In a normal high-purity III-IV semiconductor like GaAs, the electronic states in the valence bands are filled and the conduction band is empty, the two bands being separated in energy by a band gap. If free electrons are introduced in such a crystal, they will populate the electronic states of lowest energy available to them, which are in the conduction band near the band edge.

The band gap of AlGaAs is higher than GaAs, and in the absence of any doping, the band edge would be flat along the z direction (perpendicular to the surface) of the heterostructure with a step function at the GaAs / AlGaAs interfaces^[5]. How-

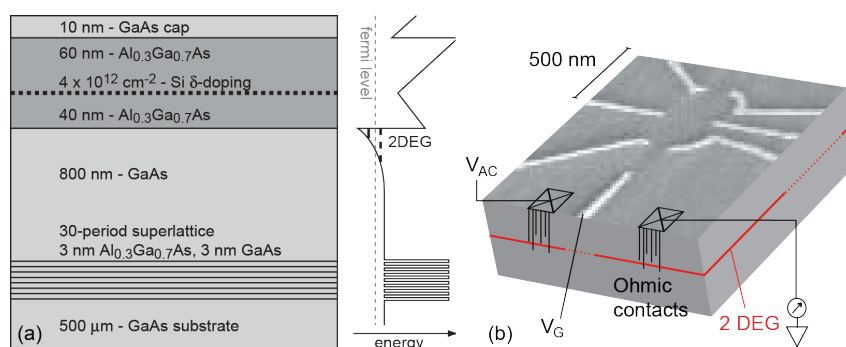


Figure 3.1: (a) Left: Schematic of the GaAs heterostructure of the G050329A wafer used to fabricate the CB7 sample. Ti/Au gates are deposited on top of the GaAs cap at a total distance of ~ 110 nm to the 2DEG which forms at low temperatures at the interface between the GaAs and AlGaAs layers. Right: The energy of the conduction band edge. The delta-layer of Si dopant atoms curves the band edge, causing a triangular potential well to form in which the 2DEG is confined. (b) Illustration of the controlled, local depletion of the 2DEG below the top gates deposited via lithographical techniques. Negative voltages are applied to these gates, electrostatically depleting the electron gas underneath. Ohmic contacts provide electrical contact to the 2DEG through the AlGaAs layer. Adapted from figure 2.2 in Christian Barthel's thesis (ref. [4]).

ever, the Si atoms in the delta-doping layer are positively charged and thus electrostatically decrease the electronic energy near it, causing curvature of the conduction band. At the GaAs / AlGaAs interface this creates a roughly triangular potential well, and since the Fermi level in the heterostructures used here lies just below the conduction band edge of GaAs, electronic states in this potential well will be populated by the free electrons. These negatively charged electrons will in turn also curve the conduction band energy, and in the bulk of the crystal the band is roughly flat. See fig. 3.1a (right) for an illustration of the band energy in the heterostructure.

Free electrons in GaAs behave approximately like free particles subject to the Schrödinger equation, although with an effective mass m^* determined by the host material rather than the free electron mass m_0 . As free particles are confined, their states become increasingly quantized. Near the interface, the electrons are now confined along the z -direction of the heterostructure, whereas they remain free in the lateral directions. If the growth parameters of the heterostructure were just right, only one eigenstate of the z -component of the Schrödinger equation is below the Fermi energy, so that all excited states are empty at cryogenic temperatures. The result is that the electrons in the triangular potential well behave as two-dimensional objects, hence the name "2-dimensional electron gas", or 2DEG.

The 2DEG is a versatile quantum system, involved in several Nobel prizes for the discovery of the Quantum Hall Effect^[23, 29] as well as High Electron Mobility Transistors^[31] (HEMTs). The geometry of the electron gas can be further confined electrostatically, enabling the formation of quantum dots, able to hold single electrons and enable electron spin-based quantum information processing. Electron beam lithography is used to define electrodes on the top of the heterostructure, referred to as *top gates* or *depletion gates*, with a lateral resolution of only tens of nm. The experimentalist can then custom-engineer a quantum system for the purposes needed. The two sets of such devices reported on in this thesis will be described below.

Okulova's devices were so-called *15-in-a-row* devices, arrays of 15 quantum dots in series potentially useful for a wide range of experiments. It was on one of these devices that the majority of experiments during the experimental run were done.

3.2.1 CB7 devices

Christian Barthel's devices were used in his Ph.D. thesis^[4] to demonstrate control and fast electrical measurement of electron spin qubits in double quantum dots (DQDs), and later by Higginbotham *et al.* who demonstrated improved coherence time of the qubit with the quantum dots being operated in the multi-electron regime compared to the single-electron case^[12].

The CB7 sample is a single chip cleaved from the 050329A wafer, grown by Micah Hanson in the Gossard group at U. C. Santa Barbara. This wafer has a carrier density $n = 2 \cdot 10^{11} \text{cm}^{-2}$, and mobility $m = 2.0 \cdot 10^5 \frac{\text{cm}^2}{\text{Vs}}$. The sample contains a 4x4 array of lithographically identical devices, several of which were explored, and some of which survived the transport from Harvard to Copenhagen. The devices are designed as double quantum dot (DQD) devices, two adjacent quantum dots with tunable coupling, defined in the 2DEG situated 110 nm below the surface of the substrate.

On either side of the DQD system are charge sensors - a quantum point contact (QPC) on the left², and a sensor quantum dot (SQD) on the right, though one of the gates confining the sensor dot can be used as a QPC if necessary.

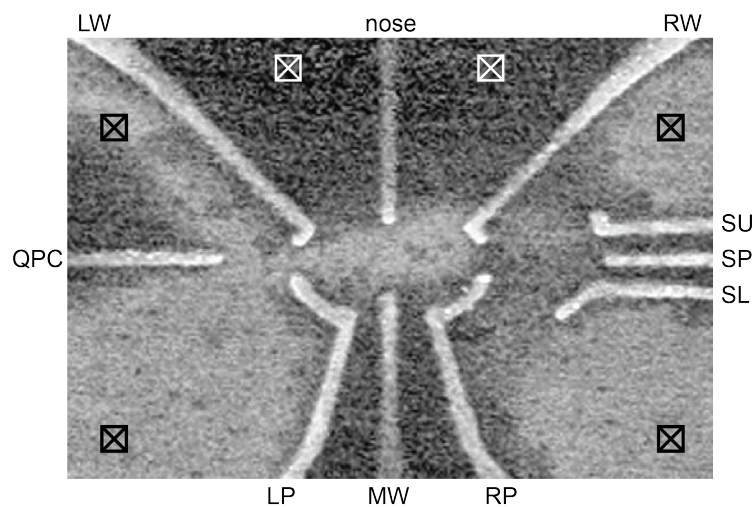


Figure 3.2: SEM image of one of the lithographically identical CB7 devices, specifically CB7 2_1. The black residue is of unknown origin. Black squares with crosses denote ohmic contacts to the 2DEG. The labels on the gates are shorthands for: Right/Left Plunger; Middle Wall; Right/Left Wall; Sensor Upper/Plunger/Lower; Quantum Point Contact

²"Left" and "right" are somewhat arbitrary; the orientation is based on whatever is most aesthetically pleasing.

3.2.2 NO7 devices

The primary novel device measured on during this Master's project is called **NO7a**, one of the six devices in the NO7 batch made by Nastasia Okulova at Center for Quantum Devices in 2013. The design was intended to be versatile system useful for a wide range of experiments. Apart from the asymmetric double quantum dot systems investigated during this project, the device has been configured with success to host multiple triple quantum dot systems simultaneously. A single device can be configured in many ways depending on how the experimentalist chooses to bond the electrical connections to it, and the many available dots provides some fault tolerance as a subset of the gates can be chosen to conduct the experiment.

The same general design has been used on all six devices in the NO7 batch, named *NO7a*, *NO7b*, etc., although in three scaling factors. Devices *a* and *d* constituted the base design with the smallest distance between top gates, by definition at scale factor 1. Devices *b* and *e* had dimensions of factor 1.2, ie. 20% larger, and *c*, *f* and had a scaling factor of 1.5. The base design with relevant dimensions can be seen in figure 3.3.

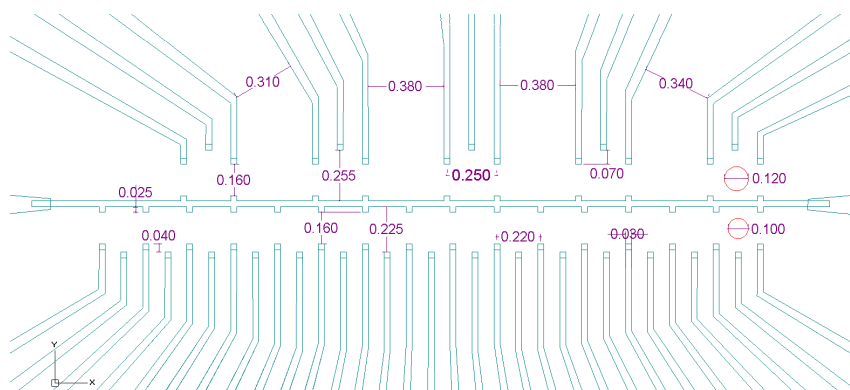


Figure 3.3: Screenshot of the DesignCAD file used in the fabrication of NO7a and NO7d, with relevant device dimensions indicated in units of μm . The horizontal gate in the middle is referred to as the **backbone**. Below are gates intended to confine quantum dots for use as qubits; above the backbone are gates intended to form slightly larger quantum dots for use as **sensor dots** (SQDs). Rough estimates of the approximate dimensions of the quantum dots are shown in the red circles. The inter-gate distances were scaled by factors 1.2 and 1.5 in devices NO7b,d and NO7c,f respectively.

These devices were made on chips cleaved from the wafer M8-27-13.1 grown by Michael J. Manfra of Purdue University. This wafer has a carrier density³ of $n = 2.5 \cdot 10^{11} \text{cm}^{-2}$ and a relatively high mobility of $m = 2.3 \cdot 10^6 \frac{\text{cm}^2}{\text{Vs}}$, an order of magnitude above that in the wafer used for CB7.

The GaAs / AlGaAs interface where the 2DEG resides is 57 nm below the sur-

³Carrier density and mobility are "dark" values, meaning that the wafer was not illuminated during the measurements which would alter the values by exciting electron/hole pairs.

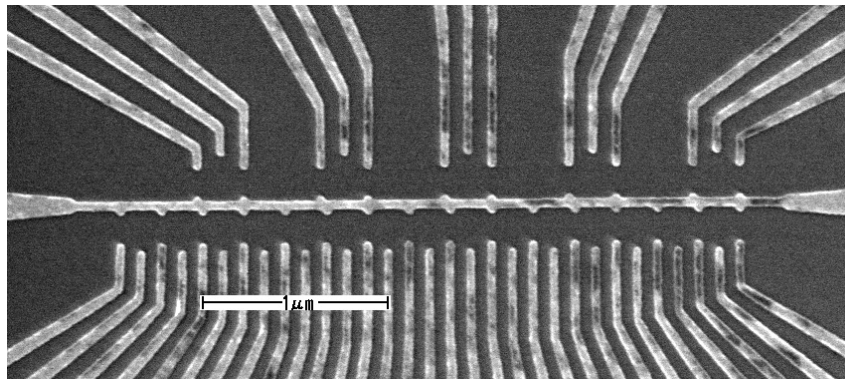


Figure 3.4: SEM image of the fabricated NO7a device. Image was taken with an Elionix ELS-7000 Electron Beam Lithography system. The five quantum dots on top in the picture are sensor quantum dots (SQDs), referred to as S1, S2 etc. from left to right. The gates confining the SQDs are referred to as S1L, S1P, S1R, S2L, etc. The row of quantum dots below are similarly referred to as Q01, Q02 etc. The gates below the backbone confining the quantum dots are referred to as Q01W, Q01P, Q02W, Q02P etc.

face, which is considered shallow. The potential benefit of such a wafer is that the gates are closer to the 2DEG, resulting in stronger electrical coupling and thus lower gate voltages necessary for depletion of the electron gas underneath. The downside is a proportionally lower tunneling distance from the gates to the 2DEG, which could result in higher gate leakage, and indeed it was found that the device was noisy unless bias cooled (see section 4.1) with comparatively high positive voltages on the gates (+350 mV).

Given the device dimensions of NO7a as shown in figure 3.3, a rough estimate of the expected effective dimensions of the quantum dots can be made, on the order of 100 nm for the quantum dots and slightly larger for the sensor dots, though it should be noted that the quantum dots formed during an actual experiment will not be as benignly symmetrical as indicated in the figure. While the gates have a width of 30 nm in the design file, the width of the fabricated gates can be expected to be wider, and size of the depleted region underneath the gates will vary depending on the voltage applied on them.

3.3 Sample board

The devices measured were mounted on Mayo Board V1R1 sample holders (see fig. 3.5). These are printed circuit boards (PCBs) which were manufactured by Mike Shea of the Mayo Clinic in 2012, designed to fit into the slug designed by Oxford Instruments which mates to the cryostat cold-finger (see next section). The boards are equipped with 51-pin nano-D connectors for DC lines, of which 48 are addressable, and 11 SMP coax connectors.

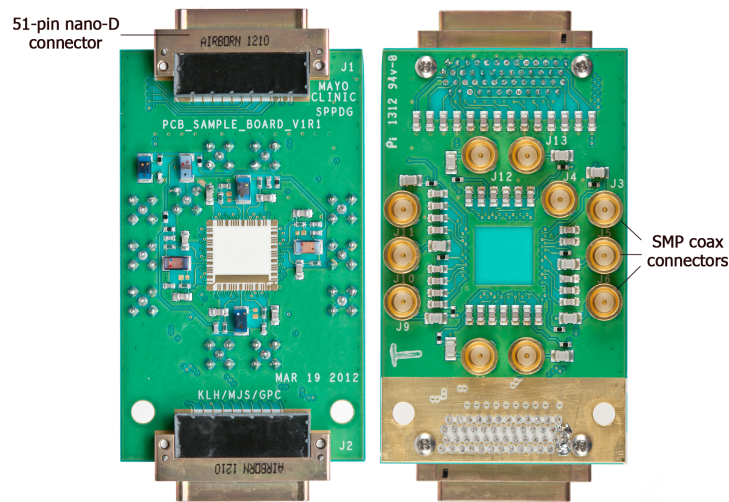


Figure 3.5: Mayo Board V1R1. Left: Front of board. Sample is mounted in the square in the middle. Right: Back of board. Semi-rigid copper coax cables connect to the circular SMP connectors on this side.

The samples were glued onto the white square in the middle with either silver paint or photoresist (AZ4533). Silver paint was the traditional adhesive of choice; photoresist was tried as a substitute due to concerns of the layer of silver paint potentially acting as a capacitor and unnecessarily adding stray capacitance to the electrical system, ideally kept to a minimum as it interferes unpredictably with the rf properties of the device. However, it was observed that this method sometimes resulted in bubbles forming in the resist, slightly lifting the sample chip and generally not providing a very stable adhesion, so this alternative is not recommended.

With the sample attached to the Mayo board, thin aluminum wires are bonded from the gold bond pads on the sample board to the contact pads on the sample using a wire bonder, an apparatus that allows the user to manually place the wires with high precision. The narrow bond pads are routed on the board to the DC lines addressable via the 51-pin nano-D connector, and the wire bond thus facilitates the electrical connection between the microscopic gates on the device and the electrical wiring accessible to the experimentalist. In addition to the DC pads, there are also wider bond pads. Ten of the coaxial connectors are routed to these through bias

tees, circuit elements that combine RF and DC signals, enabling high-frequency RF signal at a certain DC offset to be applied to a chosen gate on the device. This is essential for fast qubit control.

Additionally, four of the wide bonding pads are connected to the so-called RF Sense network, which consists of four RLC circuits ("tank circuits"), each one with a characteristic resonant frequency. These are intended to enable fast (sub-microsecond) measurement of up to four charge sensors on the device simultaneously via *reflectometry*, explained in more detail in section 4.3. The four tank circuits are connected in parallel on the *reflectometry line* going to the last available coax connector, which connects the device with the greater reflectometry circuit, see fig. 3.10. Each tank circuit is connected to an "RF sense" bonding pad, which are bonded to ohmic contacts on the sample. The resistive element R in the RLC circuit is then provided by a charge sensor in the device, eg. a QPC or SQD (see section 4.2).

The resonant frequency f_0 of an RLC circuit is given by:

$$f_0 = \frac{1}{2\pi\sqrt{LC}} \quad (3.1)$$

Briefly, reflectometry is the technique of measuring the reflection of an AC signal at or near this frequency, caused by two connected circuit elements having different (or "mismatched") impedances. The characteristic impedance of rf lines is standardized at $Z_0 = 50\Omega$, and for impedance matching to occur a tank circuit must have equal impedance, at which point there is full transmission of the signal power to the load ie. no reflection. The greater the mismatch, the greater the portion of signal will be reflected. The impedance Z of an RLC circuit for an ac signal at the resonant frequency f_0 is approximately^[4]:

$$Z \sim \frac{L}{RC} \quad (3.2)$$

L is the inductance, provided by a surface-mount inductor in the tank circuits on the Mayo board. R is the resistance, which is the variable of experimental interest, and C is the capacitance. By default, the Mayo boards are fitted with *varactors* (capacitors with variable, voltage-controllable capacitance) on the tank circuits, the idea being to enable control of C in eqs. 3.1 and 3.2, but for our experiments these varactors were removed from our sample boards as the added, although controllable, capacitance was counterproductive to reaching the impedance matching condition, as the stray capacitance from bond pads, bond wires, 2DEG channels etc. was already comparatively high. The parasitic capacitance is beyond direct experimental control, but can be kept low by keeping bond wires short, avoiding crossing of bond wires and routing the wires away from conducting planes.

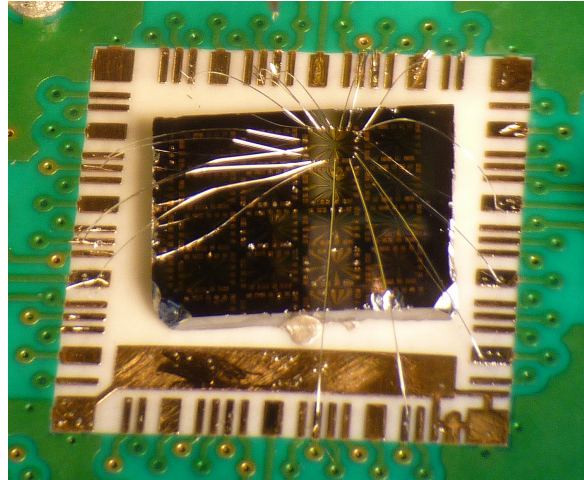


Figure 3.6: Sample CB7 bonded to a Mayo V1R1 sample board. The thin Al wire bonds connect the bond pads on the sample board to the bond pads on the chosen device, here CB7_3_4, providing the electrical access to the depletion gates and ohmic contacts. The wide bond pads are either routed to coax lines through bias tees ("fast lines"), or to the RF Sense circuit used for reflectometry.

We also replaced the standard surface-mount inductors in the tank circuits with others of higher inductance, which allows a higher capacitance for impedance matching at a given resistance in the RLC circuit given eq. 3.2. Furthermore, higher inductance shifts the resonant frequency f_0 down as per eq. 3.1, which was beneficial in regards to using carrier frequencies within the bandwidth of the RF components available for the external demodulation circuit used for reflectometry readout shown in figure 3.12. The standard inductors with inductances 68, 150, 270 and 620 nH were replaced with inductances of 470, 620, 820 and 1200 nH. The inductors were from a CoilCraft sample kit. The Mayo boards modified in this way have serial numbers #24 and #25, and we refer to them as Mayo24_mod2 and Mayo25_mod1 respectively.

It is important to note that, when bonded to the sample board, excessive caution must be exercised to keep the contacts grounded at all times, as the nano-scale metal contacts are very sensitive to electrical discharges. Many hours of fabrication have been lost, and approximately as many experimentalist tears shed, due to "blown" devices caused by insufficient experimentalist paranoia.

With the device bonded to the sample board, the board is then mounted into an Oxford Instruments "51-14" puck (see fig. 3.7), which can be loaded into the cryostat through the load lock.

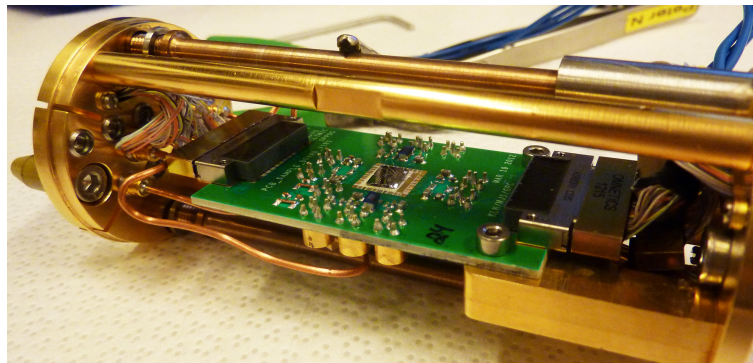


Figure 3.7: Mayo board with sample bonded, mounted in 51-14 puck. Before loading in the fridge, the outer shield of the puck is also attached. See figure 3.4.4 for an image of the puck attached to the cold finger on the cryostat.

3.4 Cryostat

To store quantum information in spin states of electrons it is necessary to cool the system to cryogenic temperatures for a number of reasons. Low temperatures are necessary for a 2-dimensional electron gas (2DEG) to form in a semiconductor heterostructure, which is a fundamental necessity for forming lateral quantum dots. Beyond that, the thermal energy should be low enough that electrons are not thermally excited between energy levels, and the energy levels are themselves subject to thermal broadening. Additionally, the spin relaxation time T_1 of a system of confined electrons is inversely proportional to temperature^[10], meaning that low temperatures are necessary in order to obtain long decoherence times.

To achieve the necessary temperatures, we employ a Triton™ 200 helium dilution refrigerator system provided by Oxford Instruments, which enables cooling of samples to about 20 mK, corresponding to a thermodynamic energy of $1.7 \mu\text{eV}$. This machine also contains a vector magnet capable of generating magnetic fields in arbitrary directions on the sample, up to 6 Tesla in the vertical axis and 1 T in the horizontal axes. The operating principles of this cryogenic technology will be briefly introduced.

There are two methods of cooling operating in the cryostat. The bulk of the heat removal from room temperature to cryogenic temperatures is achieved with a Pulse Tube Refrigerator (PTR), which removes heat by expansion of helium gas. The final cooling is done with helium dilution refrigeration, in which heat is removed by diluting liquid ^3He into liquid ^4He . A helium compressor circulates helium through the dilution unit (DU) where the cooling takes place.

The two upper-most stages are cooled by the pulse-tube cooler, and are referred to as PT1 and PT2, PT1 having an operating temperature of ~ 55 K, and PT2 of about 4 K. The next three stages are the *still plate*, the *100 mK plate* and the *mixing chamber plate* (or "M/C plate"). The mixing chamber plate has a mixing chamber where the helium dilution cooling takes place, described in section 3.4.3.

3.4.1 Cryostat layout

Physically, the cryostat (or "fridge" in the lab vernacular) consists of several stages of progressively lower temperatures, enclosed in a cylindrical high vacuum chamber. High vacuum is needed to prevent thermal exchange with the environment, and the pressure inside the chamber is ideally lower than 10^{-5} mbar. The vacuum cans are suspended from a shock-damped top plate, which is at room temperature.

There are several layers of heat shields protecting the inner layers from thermal radiation. The heat shields are brass cylinders mounted on the still plate, PT2 plate and PT1 plate, and are each at thermal equilibrium with these. Counting the outer vacuum chamber cans, there are 4 layers of metal between the outside environment and the mixing chamber. The layers consist of one to three cylinders (known locally as "cans") and all in all a great deal of time has been spent removing and assembling these in times of fridge-troubleshooting.⁴

The plates visible in figure 3.8, heat shields etc. are enclosed in a vacuum chamber sometimes referred to as the OVC, which stands for *outer vacuum chamber*, a relic from the ancient past (pre-2002^[28]) when cryostats generally had two vacuum chambers. The *inner vacuum chamber* (IVC) was necessary for using cryogenic liquids (liquid nitrogen & helium) for precooling the helium mixture for the dilution unit. Systems using this method are referred to as "wet" dilution refrigerators, and in contrast the fridges used in QDev are "dry" or "cryogen-free" dilution refrigerators.

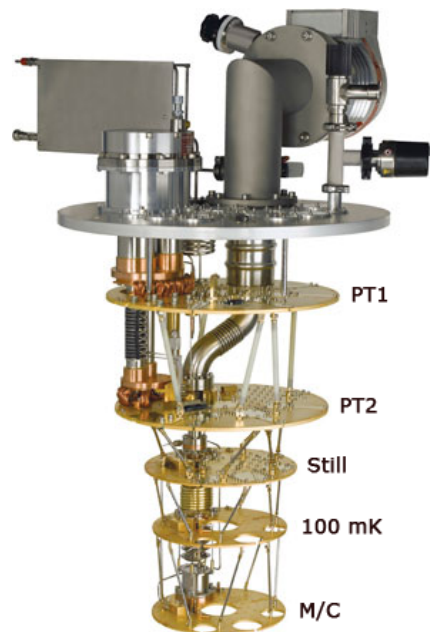


Figure 3.8: "Naked" Triton 200 helium dilution refrigerator. Vacuum cans, thermal shields, magnet and custom electronics not shown.

⁴Legends say that Andrew Higginbotham once closed a fridge unassisted, as he was the last man standing in the lab that evening and wanted to cool down overnight. While an impressive feat of strength and experimental determination, he says he doesn't recommend it.

3.4.2 The Pulse Tube Refrigerator

The cryostat employs a Cryomech[®] PT410 Two-Stage Pulse Tube Cryocooler which removes heat via the compression and expansion of helium gas.^[18] The cooling engine consists of three parts; a compressor package, a rotary valve, and the cold heads.

The helium compressors for the cryostats in QDev are situated in the chiller rooms, also known as chases, where heat from compression (and ultimately the cryostats) is removed via water cooling.

The rotary valve, mounted on top of the cryostat, periodically switches the helium connection to the cold head between the high and low pressure level of the compressor during the compression/expansion cycle, which is the source of the *tchk, tchk* noise in the lab.

The cold heads are located inside the vacuum chamber of the cryostat. There are two stages of cooling, with one stage precooling the helium gas to the other. The two cold heads are thermally connected to the PT1 and PT2 plates via copper braids in order to reduce the transfer of mechanical vibrations from the PTR to the cryostat.

The PTR system is able to cool the cryostat (below the PT1 stage) to about 4 K. This is sufficient to condense the helium gas used for dilution refrigeration into a liquid state. The electromagnet used to apply magnetic fields on the sample is superconducting and therefore needs to be kept below its critical temperature, and is mounted on the heat shield connected to the PT2 plate.

3.4.3 The Dilution Unit

Dilution cooling occurs due to the *enthalpy of mixing* of diluting ^3He into ^4He ^[20], which happens in the *mixing chamber* in the cryostat mounted on the M/C plate.

Below approximately 0.9 Kelvin a mixture of ^3He and ^4He will separate into two phases: a "concentrated phase" consisting of mostly of ^3He , and a "dilute phase" composed mostly of superfluid ^4He with a small percentage of ^3He depending on the temperature. At very low temperatures (below 100 mK) the concentrated phase contains almost 100% ^3He , with about 6.6% in the dilute phase.^[30]

If the dilute phase is pumped on, ^3He will boil off preferentially to ^4He . To restore equilibrium, ^3He from the concentrated phase will diffuse into the dilute phase, and in crossing the phase boundary will extract heat from the mixing chamber, which is thermally connected to the sample. Temperatures as low as 18 mK can be reached in the cryostat using this method. The theoretical limit is lower, but is subject to engineering challenges. The dilute-phase mixture is collected in the *still*, mounted on the still plate, and pumped on through a turbopump mounted on top

of the cryostat.

The $^3\text{He}/^4\text{He}$ dilution depends on a steady supply of cold ^3He on the concentrated-phase side of the mixing chamber. An external helium compressor (made by KNF[®]) provides high-pressure helium gas mixture, which is condensed in a Joule-Thompson stage, where the gas is throttled under efficient heat exchange and thus liquefied. The condensed mixture is led to the mixing chamber through various ingenious heat exchangers in which the mixture is pre-cooled by the evaporated ^3He . The components below the Joule-Thompson stage are collectively called the *dilution unit*.

3.4.4 Sample loading

A big advantage of the Triton[™] 200 system is that it allows the user to load a sample without having to warm up the cryostat to room temperature. This is achieved with a load lock system at the bottom of the fridge. The user mounts the sample puck into a puck loading stick, which is then attached to the load lock with four screws and subsequently evacuated with a turbopump. When the pressure in the load lock is below 10^{-4} mbar, the user can gently slide the sample puck through some flaps in the heat shield, and attach (or detach) the puck onto the *cold finger* of the cryostat. The cold finger is attached to the mixing chamber plate, and the cold fingers and pucks in the lab have mating flanges which connect the rf coax lines and DC looms of the cryostat to the sample puck.

Some *fingerspitzengefühl* is required when loading or unloading a fridge. You are operating in the dark, and it helps to have a solid mental image of what is going on around the sample puck in relation to drive rods, hex keys and mounting screws. While it is intimidating at first, aptitude comes with practice. It is important to collect the helium mixture into the tank before starting any loading or unloading procedure - bringing a room-temperature chunk of metal into thermal contact with a 20 mK mixing chamber will impart a significant heat load, and the helium mixture will evaporate, possibly resulting in dangerous overpressure. Verify that the magnetic field is ramped to zero before loading or unloading. Make sure that you and the sample are grounded at all times during the procedure to avoid blowing the device.



Figure 3.9: Sample puck loaded onto cold finger on cryostat with vector magnet off.

3.5 Electronics

With a quantum device firmly loaded into the cryostat, all interaction with the sample is electrical in nature. Multiple obstacles must be overcome, as a very high degree of sensitivity is needed to distinguish single electron charges. This section provides an overview of the electrical setup of the experiment, as well as the electronic equipment used. See figure 3.10 for a diagram of the electronic circuitry.

The electronics used can be roughly divided into two subcircuits; the DC lines and the RF lines. On the sample, a direct current (DC) voltage is applied to the gates in order to electrostatically define the quantum system. It is also useful to measure low-frequency (<1 kHz) currents through the device, such as the transport of electrons through one or more quantum dots. Furthermore, in order to initialize, operate and measure spin qubits, high-frequency (RF) electrical signals are applied and modulated by various waveform generators, amplifiers etc., explained in section 3.5.2.

3.5.1 DC lines

In the Triton 200 cryostat used for the experiments, a total of 48 DC lines⁵ are available, routed through two twisted-pair looms of 24 lines each. The looms are combined in the cold finger to fit a 51-pin nano-D connector in the cold finger of cryostat, which connects through the sample puck to the nano-D connector on the sample board. The DC lines in the cryostat are led through two electrical filters mounted on the mixing chamber, in order to reduce high-frequency electrical noise as well as thermalizing the room-temperature electrons to cryogenic temperatures before reaching the sample. Each of these filters consist of copper enclosures with a 4-layer printed circuit board inside, in which surface-mount electrical components are soldered on.

In order to cool the electrons in the DC looms connected to room-temperature circuitry, the looms are led through (or rather around) a set of **bobbins**, copper cylinders with the looms tightly spooled around them to provide thermal contact. These are situated on the mixing chamber plate, and should therefore have a temperature of around 20 mK when the fridge is cold.

The *RC filters* consist of a surface-mounted 80 MHz low-pass filter integrated circuit (Mini-Circuits LFCN-80, "pi filters") for each line, connected in series with two RC circuits, with $R = 2 \text{ k}\Omega$ resistors and $C = 2.7 \text{ pF}$ capacitors to ground. This gives an RC time⁶ of $5.4 \mu\text{s}$.

⁵Assuming no electrical errors in the cryostat - sometimes a bad assumption.

⁶When a square voltage pulse is applied to an RC circuit, the RC time, τ , is the time it takes before the voltage on the output is within $1/e$ ie. 63.2% of its final value.

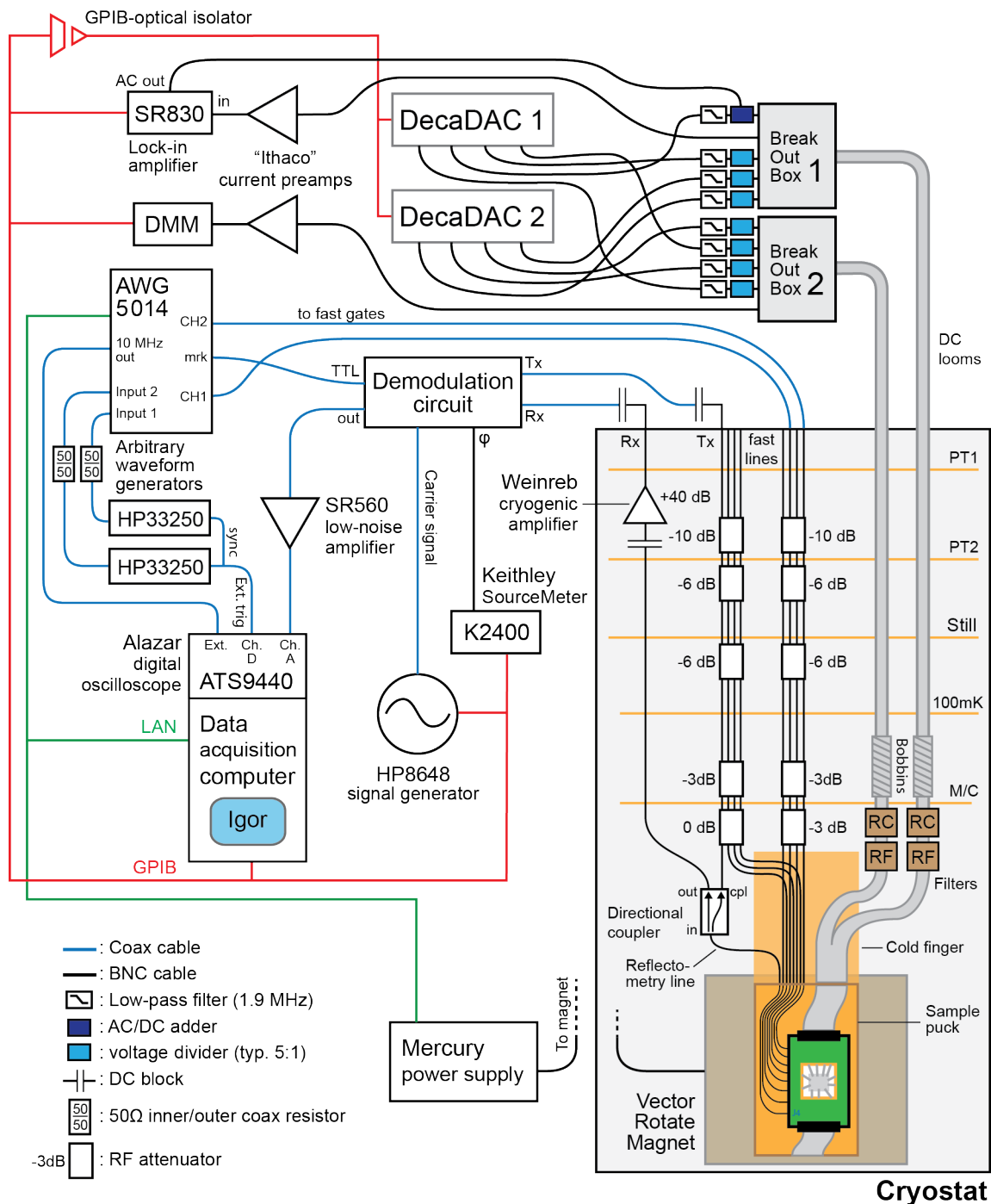


Figure 3.10: Electronic circuit of the experimental setup. The instruments can be seen in figure 3.11

The benefit of the RC filters is that they absorb (most of) the filtered signal rather than reflecting it, however very high frequency noise (>10 GHz) is not entirely suppressed. For additional filtering *RF filters* are used, in which each line passes through three additional Mini-Circuits *pi filters* in series with different cutoff fre-

quencies, namely 80 Mhz, 1.45 GHz and 5 GHz from input to output (Mini-Circuits LFCN-80, LFCN-1450 and LFCN-5000). These filters reflect high-frequency noise beyond the domain of the RC filters.

By analyzing the width of a Coulomb peak in the charge transport through a quantum dot, it is possible to estimate the effective electron temperature in the sample. Applying a gaussian fit to one such peak, an upper bound for the electron temperature was found at 0.3 K. This is somewhat higher than electron temperatures measured in a similar dilution refrigerator (~ 150 mK as measured by C. Barthel^[4]). The electron levels are broadened in energy thermally and by coupling to the leads, and hopefully the peak analyzed was predominantly broadened by coupling and not electron temperature. Regardless, the incumbent fridge user Andrew Higginbotham suggested reordering the filters (input - RC - RF - bobbin - sample) to optimise the thermalization.

Break-out boxes

The break-out boxes (or BOBs) is the experimentalist's access to the DC lines in the fridge and ultimately the sample. They are mounted on a rack outside the fridge, and are each connected to the DC looms via 24-pin Fischer connectors to a turret on top of the cryostat. Each line on a BOB has a BNC connector and three settings controlled with a switch: *bus*, *direct*, and *ground*. *Direct* simply provides a direct connection between the BNC connector and the DC line. The *bus* setting connects the line to a bus line, shared between all lines on the *bus* setting in the BOB, which also accessible through a separate BNC connector. In our setup, the bus lines on each BOB was connected through a BNC cable through these bus connectors. The *ground* setting shorts the line to ground. The break-out boxes are grounded to the same ground as the cryostat.

DecaDACs

The voltages applied to the device gates and ohmics are mainly (but not exclusively) supplied by digital-to-analog converters of the "DecaDAC" type made by Jim McArthur at the Harvard Electronic Instrument Design Lab. Each DecaDAC has 20 channels, each capable of supplying up to ± 10 V. The output of each channel is controlled by the user through Igor, which communicates with the DecaDAC through a fiber-optic GPIB interface. The DAC channels are connected to a chosen connector on a break-out box through BNC cables, resulting in a tangled, though impressive-looking, mess of cables between the DACs and the BOBs.

Each channel has three settings; ± 10 V, 0 to +10 V and -10 to 0 V. The DecaDACs have 16-bit resolution, meaning that the voltage range is divided into 65536 bins,

giving a resolution of 0.153 mV between voltage steps (if on either of the two latter settings). To increase this resolution voltage dividers are used between DAC and BOB, typically with a voltage division of either 5:1 or 6:1, giving a final voltage resolution of approximately 30 μ V. Furthermore, BNC low-pass filters are used to reduce high-frequency noise.

When biasing quantum dots, the voltage supplied to the source-side of the dot frequently needs to be of much lower voltage, and higher resolution is more important. 1000:1 voltage dividers were commonly used for this application.

Ithaco current preamplifiers

In the experimental setting we frequently want to measure a minute current, eg. the current running between source and drain of a quantum dot. To detect these very small currents, we rely on current preamplifiers of the Model 1211 type by DL Instruments, a company formerly named Ithaco Precision Instrumentation Division⁷, hence the nickname of "Ithacos" for the preamps. The function of these devices is to convert measured current to a voltage, which is easily measured with a digital multimeter (DMM).

The Ithaco preamplifiers have a variable sensitivity setting ranging from 10^{-3} to 10^{-11} ampere/volt. For our purposes we most frequently used a sensitivity of 10^{-7} or 10^{-8} A/V, giving good signal-to-noise without overloading in the nanoampere to picoampere range.

There are three types of outputs on the preamplifiers: 50 Ω matched, 600 Ω matched and X-1, which is amplified but unfiltered output. On the former outputs, a variable rise-time (RC) filter is used, which is useful for averaging out high-frequency noise, giving a smoother reading. For current measurement with DMMs, rise-time constants of 30 to 100 ms were used, with the DMM connected to a 50 Ω output. The multimeters used were HP 34401A Digital Multimeters.

SR830 Lock-In Amplifier

Lock-in amplifiers are ingenious devices which allow the user to measure the attenuation and phase-shift of an applied signal of a specific frequency. This is useful if the signal to be measured is noisy, since the lock-in amplifier (commonly referred to simply as "lock-in") picks out only the frequency of interest. The lock-in amplifiers used predominantly in Center for Quantum Devices are SR830 models from Stanford Research Systems^[26].

The lock-in generates a reference signal of a chosen amplitude and frequency, and measures the amplitude of signal received through its input channel at that

⁷<http://dlinstruments.com>

particular frequency using *homodyne detection*. This can be used to measure the conductance through a charge sensor in a device, ie. a QPC or SQD. Homodyne detection is also used in the demodulation circuit to enable fast readout of charge sensors, described in section 4.3.2.

Due to the RC filtering of the DC lines in the cryostat, relatively low frequencies must be used for the reference signal. For the most part we used 137 Hz. A prime number away from a multiple of 50 is recommended, to avoid interference with the ubiquitous 50 Hz noise.



Figure 3.11: Image of the room-temperature electronic devices used in the experimental setup.

3.5.2 RF lines

Generally when manipulating and measuring qubits, various techniques involving high-frequency electrical signals are used, electron spin qubits being no exception. For our experiment we have used RF signals for two purposes. One being fast control of the voltage on plunger gates, to quickly change the charge state of the quantum dots, achieved with arbitrary waveform generators (AWGs). The other being fast readout of the resistance of a charge sensor via *reflectometry*, a technique that will be discussed in detail in section 4.3.

Coax lines in cryostat

The Triton 200 cryostats come with two circular line-of-sight (LOS) ports, visible in figure 3.8, which in our setup hold two *coax inserts* of 8 coax lines each. The coax inserts consist of shorter, semi-rigid coax cables connecting plates clamped to each of the stages in the cryostat (PT1, PT2, etc.). Except at the PT2 and 100 mK plates, each plate has one or two rf attenuators. The purpose of these is primarily to thermalize the electrons in the coax lines to prevent heating and thermal noise during measurement, as well as lowering the input power of the rf signals applied to avoid overloading the sensitive nanostructures, which could result in a blown device.

The type of coax cables used, as well as the configuration of attenuators, differ between the two coax inserts (see fig. 3.10). The inner coax insert, 65 mm in diameter, has SSS/SS coax cables⁸ between top plate and PT1 stage, and NbTi/NbTi from PT2 plate to mixing chamber plate, and the total attenuation on these lines is -28 dB. The outer insert, 50 mm in diameter, has slightly inferior SS/SS coax cables from top to bottom, and a total attenuation of -25 dB. Both inserts have Cu/Cu semi-rigid coax cables connecting from the ports at the mixing chamber plate to the cold finger.

There are 14 SMP bullets on the cold finger mating to the sample puck. Of these, 13 are used as *fast lines*, simply connecting the SMA connectors on the top of the fridge to the SMP bullets at the cold finger. The last is the *reflectometry line*. This is part of the reflectometry circuit used for readout of charge sensors on the device. This line connects to a **directional coupler**⁹ mounted below the mixing chamber plate, which is used in a slightly counter-intuitive way. The usual mode of operation of a directional coupler is to insert a signal on the input port, have the majority of the signal power transmitted to the output port, while diverting a minor fraction of the signal to the coupled port for analysis purposes.^[17] However, we are

⁸Silver-plated stainless steel on the inner conductor, stainless steel on the outer.

⁹Mini-Circuits ZEDC-15-2B

interested in applying an electrical signal to the reflectometry line and measuring the reflection of this signal with as little loss as possible.

This is achieved by using the coupled port as the electrical input via the **Tx line** on the outer coax insert, which couples to the input port of the directional coupler at the cost of -14.7 dB attenuation¹⁰. The signal travels from the input port to the reflectometry circuit of the sample, where some portion is reflected depending on the state of the charge sensor, described in section 4.3. The reflected signal then travels back to the directional coupler, where it is transmitted with little loss to the output port, and from there to the **Rx line** also situated in the outer coax insert. The attenuators have been replaced with 0 dB "dummy" attenuators on the Rx line, since it is useful to recover as much as the reflected signal signal as possible. The reflected signal is passed through a **DC block** on the PT2 stage¹¹, and amplified with a **Weinreb cryogenic amplifier** also thermally connected to the PT2 stage.

Arbitrary waveform generators (AWGs)

Where traditional signal generators are only able to generate electric signals of particular waveforms, ie. sine waves, square waves, sawtooth etc., arbitrary waveform generators, often referred to as AWTs or *arbs* are able to generate customized waveforms. Several of these were used in the setup, of which the most versatile was the **Tektronix AWG5014**, which can output customized waveforms at a maximum sample rate of 1.2 GS/s. It can store a number of waveforms which can be sequenced, allowing for advanced control such as Hahn echoes or other pulse sequences to counteract dephasing of a spin qubit^[11]. A sequence of waveforms can be uploaded remotely via ethernet, and in our setup this functionality has been integrated into Igor. This allows experimental control of gate voltages on a very short (≈ 1 ns) timescale, provided the device gate is bonded to a fast line on the Mayo board.

Another type of AWT used during this experimental run was a pair of **Agilent HP 33250** Function / Arbitrary Waveform Generators. While also capable of outputting arbitrary waveforms, the lower sample rate and waveform length (200 MS/s and 16.4 Kpts respectively) meant that they only saw use as function generators, a role which they serve well. Addressable via GPIB, they are integrated into the experimental control routines to deliver sawtooth waveforms of arbitrary frequency, amplitude and DC offset. The outputs from two synchronized HP 33250 AWTs were connected to the input channels of an AWG5014, which superimposed its own waveforms on the signals which were led to coax lines on the cryostat ul-

¹⁰In the frequency range of interest to us, ie. few hundreds of MHz.

¹¹This component eventually developed an electrical fault at cryogenic temperatures, see appendix A.

timately connecting to gates on the device, used for rapidly pulsing a particular DQD between different charge states.

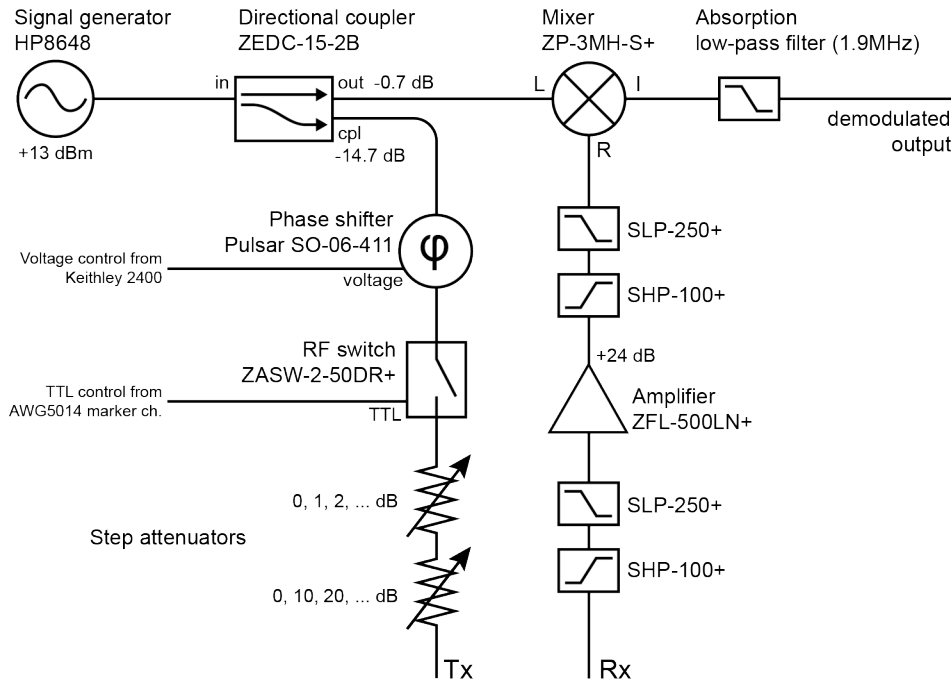


Figure 3.12: Diagram of the demodulation circuit used in reflectometry.

3.5.3 Demodulation circuit

The demodulation circuit, shown in figure 3.12, is part of the reflectometry circuit used to rapidly measure eg. the conductance through a charge sensor. A carrier signal is generated and applied to the sample via the Tx line on the cryostat. The demodulation circuit relies on mixing the carrier signal with the reflected and amplified signal from the Rx line. Due to the principle of homodyne detection described in section 4.3.2, the resulting output is an electrical waveform with a non-zero DC component proportional to the amplitude of the reflected carrier signal. The output of the demodulation can then be measured with a voltmeter, such as a DMM or an oscilloscope.

The demodulation circuit relies on various radio-frequency (RF) components with specific operational bandwidths, some narrower than others, and the particular components used for a given application must be chosen for the frequency range of interest. Our modified Mayo board has resonant frequencies roughly between 140 MHz and 230 MHz with a sample bonded, which is reflected in the choice of components for this demodulation circuit. See table 3.1 for a list of components as well as their nominal frequency ranges.

Table 3.1: Components used in various demodulation circuits in the experiment

| Part number | Function | Range (MHz) | Gain / loss |
|---------------|---------------------|-------------|--------------------|
| ZFSC-2-4 | Power splitter | 0.2 - 1000 | -3.3 dB |
| ZMSCQ-2-180 | IQ Splitter | 120 - 180 | -3 to -4 dB |
| SO-06-411 | Phase shifter | 150 - 280 | -2.2 dB |
| ZP-3MH-S+ | RF mixer | 0.15 - 400 | N/A |
| ZEDC-15-2B | Directional coupler | 1 - 1000 | -0.7 dB / -14.7 dB |
| ZASWA-2-50DR+ | RF switch | 0 - 5000 | -1.5 dB |
| ZFL-500LN+ | Amplifier | 0.1 - 500 | +24 dB |

A sine-wave signal is generated by the HP8648 signal generator at or near a resonance frequency of the sample board. The signal is passed through a directional coupler, where the main output is delivered to the RF mixer, and the coupled output is sent to the sample. The mixer has three ports, denoted L, R and I, corresponding to the *Local Oscillator* (or LO) port, *RF input* port and *Intermediate Frequency* (signal output) port. The RF mixer effectively multiplies the incoming signals, and so if pure ac signals of frequencies f_1 and f_2 are applied on the LO and RF ports respectively, the signal on the IF output ideally contains the *sum* and *difference* frequencies $f_1 + f_2$ and $f_1 - f_2$. This is called *heterodyning* (lit. "two tones"), and if $f_1 = f_2$, the difference frequency is merely a DC component and the process is called *homodyning*.

The local oscillator input power for this mixer (Mini-Circuits ZP-3MH-S+) is nominally +13 dBm, corresponding to the maximum output power of the signal generator used. The RF input is used to modulate the carrier signal and should be of lower power, around 0 dBm.

The relative phase of the LO and RF signals is important; in-phase input signals result in maximum output amplitude, which in turn is suppressed if out-of-phase. For this reason a phase shifter is incorporated into the circuit on the coupled output going to the sample, which allows for voltage-controllable phase shift and therefore tuning of the demodulated output. The phase shifter has a somewhat narrow bandwidth, and can shift the phase of the signal applied by between around 0 to 180 degrees depending on the voltage applied. A **Keithley 2400 SourceMeter** was used to control the voltage and thus phase shift. This device allows a GPIB-controllable voltage source, and furthermore acts as an amperemeter telling you the magnitude of the current being sourced, although this functionality was not strictly necessary for this specific purpose.

An alternative to using a phase shifter would be to use an *IQ splitter*, a power splitter with an *In-phase* and *Quaternary-phase* output respectively, the quaternary phase being offset by 90 degrees. Each output is then demodulated as normal. The

benefit is that one is protected from signal loss from destructive interference, as well as potentially giving phase information of the reflected signal by mapping the relative magnitudes of the two demodulated signals to a sphere. This system has been explored by Asbjørn, Asbjørn and Bjarke^[8] during an Experimental Physics project, and an IQ demodulation circuit was indeed temporarily used before opting for the simpler version shown in fig. 3.12. The problem was that the commercially available IQ splitters had narrow operational frequency ranges just out of the range of interest, and halving the reflected signal power due to power splitting was undesirable in order to achieve high signal-to-noise ratio.

It is sometimes useful to control whether or not the carrier signal is applied to the sample with a high response time. For this purpose an RF switch was used, which directs an input signal to one of two output ports depending on whether an external TTL (*transistor-transistor logic*, an electrical standard) voltage is applied to the switch. One port was used as main output, the other was terminated with a 50Ω terminator. An AWG5014 marker channel was used to control the switch, which could therefore be integrated in fast control routines. Note however that the switch employed (Mini-Circuits ZASW-2-50DR+) had a switching time of around 10 ns (according to its spec sheet), and additionally some ringing in the signal after switching was observed. For the most part, the switch was left in its *on* state.

When applying electrical signals to the 2DEG of the device, as is the case with our reflectometry circuit, care must be taken to not apply excessive power, since it could cause unwanted interference with the quantum state of the device and in the worst-case scenario damage it. For this reason, step attenuators were used as the last electrical components before the coupled output of the carrier signal entered the cryostat, allowing manual control of the attenuation. The specific attenuation was optimized for one charge sensor to yield the highest signal-to-noise ratio (SNR), at an attenuation of -42 dB, resulting in an applied power on the sample of just under -80 dBm.

3.5.4 Alazar digital oscilloscope

To achieve fast readout of the reflectometry circuit, the demodulated signal was measured with an AlazarTech ATS9440 digital oscilloscope (DSO), referred to in the lab as well as in this thesis as *Alazar*. This is a PCI-Express card which mounts directly into the data acquisition computer, providing very fast data transfer (PCIe x8 = 1.6 GB/s). The board has four analog-to-digital converters (ADCs) with high sample rate, up to 125 MS/s, although the bandwidth of the card is 65 MHz. In other words, it is able to act as an oscilloscope reading the instantaneous voltage of up to four channels simultaneously. The Alazar card interfaces directly with Igor through drivers written by James Medford at the Marcus Lab at Harvard University.

The Alazar card, in the mode in which we used it (referred to as *no pre-trigger* or NPT mode), waits for a trigger event, and when triggered starts sampling one, two or four channels for a certain amount of samples to fill one *record*. Typically, many records are acquired which can then be averaged. When a certain amount of records are recorded, it marks the filling of one *buffer*. A single buffer can store a total of around 2^{19} samples for single-channel acquisition, 2^{18} for two channels and 2^{17} samples for all four.

A buffer can consist of many samples on few records or vice versa, depending on the user's wishes. When a buffer is full, the card will start transferring the buffer while starting the acquisition of a new buffer. As many buffers can be acquired as the computer has RAM to process, but be warned - overzealous sampling with the Alazar can quickly result in an Igor experiment file of several gigabytes.

The triggering which starts an acquisition can be configured to a high degree. There are two trigger engines, and a trigger event can be caused by any logical combination of the two (such as one channel being HIGH and another being LOW, subject to customized voltage levels). In the data shown in this thesis, the trigger signal was supplied by the external trigger channel of an HP 33250 function generator, marking the start of a saw-tooth voltage sweep of a gate. After a trigger, data was acquired for the duration of the voltage sweep, giving one record (or "trace") corresponding to a gate ramp.

A 10 MHz external reference signal was supplied to the Alazar card from the AWG5014.

3.6 Data acquisition

The various instruments described in the previous section are predominantly controlled by and/or transmit measurements to a data acquisition computer. With some exceptions, the communication method used is via the **GPIB** interface, or *General Purpose Interface Bus*. Physically, this link manifests in the form of GPIB cables connecting the instruments to a GPIB card in the computer. This computer runs Igor Pro, a data acquisition and analysis platform produced by WaveMetrics, which communicates with the instruments through the interface via the GPIB protocol. In Igor, a range of *procedure files* contain functions specific to each instrument type, and are effectively the driver software. The functions can be called by the user through the Igor command line, or more likely, integrated into various experiment control routines in custom-written user procedure files.

Some instruments communicate through other interfaces, but the general principle is the same. The communication protocols, eg. Serial I/O ("COM" ports) for control of the vector-rotate magnet via the Mercury power supply, and VISA for communication with the AWG5014 and Triton control system, are integrated into Igor through plug-ins, and specific instrument drivers in the form of Igor procedure files (.ipf's) written by people in the lab enable higher-level control. In the case of communication with the Alazar card, an XOP (External Operation) extension was written for Igor by James Medford.

With many different instruments in the setup, each with many different physical parameters to read or set, keeping track of all the relevant commands would be cumbersome indeed. This was in fact the scenario in the early 2000s in the by-gone Marcus Lab at Harvard University, until a prodigious graduate student named Alex Johnson wrote a set procedures that generalized commonly used experimental routines such as instrument control, data acquisition, as well as plotting and analysis of the acquired data. The "Alex suite" has been the used by many experimentalists over the years, and since 2005 the procedures have gradually evolved as people have added functionality needed for their particular experiments. The current state is a somewhat messy genealogy, with different setups running different procedures files modified with more or less crude hacks and tweaks, to the point where functions on one setup do not translate to other setups¹².

¹²At least without some rather involved genetic engineering, which did consume a sizeable portion of time during the project.

3.6.1 Useful Igor functions

Some useful functions, the workhorses of the Alex suite, will be briefly introduced. Some more specialized Igor routines have been developed and implemented during the experimental work, which are described in chapter 5.

setval()

This function is used to set a variable, such as a voltage on a DAC output, the frequency of the output of a signal generator etc. The command has the form `setval(idstr,value)`, where *value* is the value to set, and *idstr* is an identifier string for the parameter to set. *idstr* is parsed in the `setval()` function, and the relevant, instrument-specific function is called from the function as a subroutine. For example, to set the voltage output on DAC channel 5 to -250 mV, use the command:

```
setval("c5",-250)
```

which is translated to:

```
chanramp(5,-250)
```

Thus, instead of remembering all the commands for setting different variables, it is simply necessary to remember the relevant identifier string. The `setval()` function is also extensively called from other functions in the Alex suite, enabling generic control of experimental parameters.

getdata()

Like `setval()` is the generic function to set a variable, `getdata()` is the generic function that reads and returns a value of interest. It has the form `getdata(stream)`, where *stream* is an integer. The stream is configured through the DataControl macro window, where each stream is associated with a particular data type (resistance, current, etc.), input type (DMM, lock-in, etc.), and other necessary values (eg. GPIB channel number). The settings chosen are stored in string variables, and these strings are then parsed in `getdata()` similarly to *idstr* in `setval()`. When called, `getdata(stream)` polls the relevant instrument defined in the stream, manipulates the measured value if necessary and returns the output.

For example, if one wants to measure the conductance¹³ through a quantum dot with a DMM via an Ithaco preamplifier on stream 1, the stream is configured like such:

¹³During measurements it is useful to compare resistance of a channel to the fundamental resistance quantum R_K (the von Klitzing constant $\frac{h}{e^2}$, corresponding to circa 25.6 k Ω), the resistance of a single conducting quantum channel with total transmission. Thus, the conductance of a QPC with channel resistance R is $g = \frac{R_K}{R} \frac{e^2}{h}$.

```

root:alex:S_datatype1 = "cond"
root:alex:S_InputType1 = "dmm"

```

via the DataControl window, although the strings can also be set manually. It is also necessary to specify the GPIB channel of the DMM, which is translated by DataControl to the specific GPIB address of the DMM stored in another variable. When `getdata(1)` is called the relevant strings and values are parsed, and the voltage of the DMM is read via the GPIB interface. The voltage, measured on the Ithaco output, is converted via the relevant conversion factor (eg. 10^{-8} A/V) to the measured current, which is in turn converted to the conductance and returned.

do1d()

When running an experiment, perhaps in science in general, the most ubiquitous method of inquiry is to measure one or more system variables as a function of varying a parameter. This is easily done with the `do1d()` function, which first sets the parameter through `setval()`, waits for a period to allow for response time, measures the variable(s) of interest via `getdata()`, adjusts the parameter and repeats the process.

The function has the format `do1d(idstr, start, stop, numdivs, delay)`. The function runs a series of `setval()` commands with the `idstr` parameter, with values between `start` and `stop`. It is done in as many steps as defined with the `numdivs` integer parameter. After each `setval()` call, the function waits for a period of `delay` seconds and calls `getdata()` for all active streams. The output is stored in a 1-dimensional *wave* for each stream. "Waves" are Igor's way of storing arrays of data, and can have dimensions 1 to 4. Waves additionally contain some metadata, such as units, scaling factors etc.

For example, to measure the conductance of a sensor quantum dot as a function of varying the voltage on DAC channel 5 (connected eg. to the plunger gate of the sensor) from -200 to -500 mV in 300 steps (ie. 1 mV intervals), with 10 ms wait time, the data stream is configured as shown above and the following command is called:

```
do1d("c5", -200, -500, 300, 0.01)
```

The resulting wave will have the name of `cond1c5_#`, where `#` is a serial number to distinguish the waves from each other. The serial number is incremented after each trace. In the case of more streams of data being acquired, a wave for each stream will be generated with names like `i2c5_#`, `temp3c5_#` etc.

do2d()

If one wants to measure a variable as a function of sweeping two parameters, `do2d()` is used. This function essentially takes a series of 1D traces like `do1d()`, and outputs a 2D wave. It has the form:

```
do2d(idstr1, start1, stop1, numdivs1, delay1,  
     idstr2, start2, stop2, numdivs2, delay2)
```

where each set of parameters work as in `do1d()`. The first set is the *outer loop*, referred to as the "stepped" variable, and the second set is the *inner loop*, the "swept" variable. The outer loop sets a variable, waits, the inner loop is swept, and the cycle repeats. Note that since the inner loop is swept many times whereas the outer loop is swept once, the sweep on the inner loop should be the faster of the two to complete, eg. when sweeping a magnetic field (slow) and a gate voltage (fast), the field sweep should be in the outer loop.

For example, to measure the conductance through a sensor quantum dot as a function of the voltage on the outer gates defining the SQD (the "walls"), connected to DAC channel 4 and 6, enter a command of the form:

```
do2d("c4", 0, -500, 50, 0.1, "c6", 0, -500, 50, 0.01)
```

This will result in a 2D color plot, with the conductance encoded by the color scale. An example of a 2D sweep can be seen in figure 4.3.

Furthermore, a 1-dimensional slice through a 2D plot can be obtained via the function `alexprofile()`, hotkeyed in some Igor experiment files to F5. It is also often useful to differentiate the wave along a certain axis, eg. to make changes in conductance appear more clearly. This can be done via the `diff2d()` command, hotkeyed to F9 (x-direction) and F10 (y-direction).

To learn about any function in Igor, enter the command in the command line (without executing!), right click the command, and choose "go to <function name>" from the drop-down menu. This will show you the source code.

4

Measurement techniques

With the experimental playing field accounted for, I now intend to introduce the most important methods used for preliminary testing of devices, as well as creating and optimizing quantum dots and systems composed thereof.

A fundamental prerequisite to any qubit experiment is a quantum system with the appropriate characteristics. In electron spin qubits dealt with in QDev, this means quantum dots occupied by a controllable amount of electrons, coupled to 2DEG leads and other dots with appropriate tunnel barriers. This is achieved by applying carefully controlled voltages to the individual depletion gates deposited on top of the semiconductor heterostructure some distance above the 2DEG (110 nm for CB7 devices, 57 nm for NO7 devices). This is also known as *biasing* the gates, which alters the electrostatic potential in the heterostructure underneath them and therefore the confinement potential of the electrons in the 2DEG.

There are primarily two types of gates; one type, *wall gates*, is intended to separate regions of 2DEG from each other, with a narrow channel connecting the regions with a characteristic tunnel barrier, tunable with the gate voltage. Another type of gate, *plunger gates*, are intended to be the primary control knobs for the electrostatic potential of the quantum dots, affecting the energies of the electronic states occupying them. The terminology is arbitrary as both types of gates are manufactured the same way, and in some instances a gate fulfil both roles, eg. the plunger gates of the CB7 devices.

A particular gate, beyond fulfilling its intended primary function in the 2DEG close to the footprint directly underneath it, also affects the electrostatic environment broadly in the proximity, and one therefore cannot adjust the different experimental parameters independently. A voltage difference of just a few millivolts on a wall gate between two coupled quantum dots can have a significant impact on the tunnel coupling between them, but will also affect the tunnel couplings to the leads as well as the electrostatic potential of both dots. This must then be compensated

for by adjusting the bias on other gates.

Furthermore, besides simply controlling the tunnel barriers and potentials of the quantum dots, changing a gate bias affects the general electrostatic potential landscape composing them, subtly altering their form and location. As such, increasing the negative voltage on one gate can push the quantum dot underneath closer to other gates, changing capacitances, tunnel barriers etc. It can also contort the shape of the QD, affecting electronic states and spin dynamics. The system is highly dynamic, the complexity scaling exponentially with that of the device, and combined with quantum behaviour often counter-intuitive from a classical perspective a great deal of time is spent by the experimentalist in tuning and fine-tuning the voltages on the gates.

Information about the state of the device is gained through various electrical means which will be described in the following sections. In the simplest approach, one measures the direct current (DC) transport of electrons through a region in the 2DEG, either through one or more quantum dots in series, or through a *charge sensor* structure, such as a quantum point contact (QPC) or a sensor quantum dot (SQD).

The conductance through the latter two structures is, when the device is properly tuned, highly sensitive to the local electrostatic environment, even to the point where the addition or removal of a single electron in a nearby quantum dot can be detected. Rather than measuring DC current, where each measurement takes place on a timescale of milliseconds, one can also integrate the quantum channel as the resistive element in an RLC resistive circuit and use the technique of *reflectometry* to measure charge transitions on a much faster timescale, potentially as low as a few hundred nanoseconds. This technique can be combined with fast electrical pulsing of top gates to perform high-resolution charge measurements in tens of seconds rather than tens of minutes, referred to as *fast readout*.

4.1 Cooldown tests

When preparing to cool down a sample, the first order of business is to check whether the device is functional. Having bonded the device onto a sample board and assembled the board in a sample puck, it is useful to first check that the RF response of the devices is as expected. This is achieved using the *RF puck tester* which allows the user to mount the puck and access the coax lines via SMA connectors. Each line can then be tested using a network analyzer. If a particular coax line behaves irregularly, it could indicate a faulty electrical connection in a semi-rigid coax cable in the puck assembly, or possibly a bonding error. It is useful to catch these practical mistakes early on in the process, rather than when the sample has been cooled to base temperature and carefully tuned in some configuration.

To load a sample into the fridge, the puck is loaded onto a puck loading stick (PLS, sometimes referred to as a "load lock" although this is inaccurate terminology), while making sure that both the puck and PLS are grounded to avoid static discharges between reservoirs of different electric potentials when contact is made. When the puck is securely loaded, the PLS is mounted on the bottom of the cryostat and evacuated with a turbopump. When the PLS chamber containing the puck is evacuated (typically pressures $< 10^{-4}$ mbar can be reached within ~15 minutes), the DC lines of the sample should be checked through the Fischer connectors on the PLS. While this can also be done in the RF puck tester, doing it through the PLS has the benefit that applying a voltage on the device gates has lesser risk of inadvertently destroying the device through a static discharge since vacuum is a significantly worse conduit than air. One can now test for electrical shorts between device gates. Applying a small voltage (eg. 100 mV) to a single gate with a Keithley 2400 SourceMeter (or "Keithley") and the other gates and ohmics grounded, the resistance should be several M Ω . If there is significant current being drawn, this indicates a short. If this is observed, the other gates can be successively floated while monitoring the resistance, enabling one to locate the unwanted electrical connection.

4.1.1 Bias cooling

If this test is passed, the device is ready for cooldown. Depending on the device, it is likely that one would like to apply a positive voltage to the device gates during cooldown, a technique known as *bias cooling*. Bias cooling results in some degree of "frozen-in" depletion of the 2DEG corresponding roughly to a similar negative bias applied to the gates, which is useful since it is then possible to apply less voltage on the gates when cold, reducing the leakage of electrons into the sample which causes noise^[7].

When applying the positive bias voltage the DC lines on the Fischer connectors both on the PLS as well on the top of the cryostat must be biased simultaneously, taking care that the break-out boxes are in matching states and that no ohmics will be biased. Typically a Keithley is used to apply the bias since it can simultaneously measure the leakage current. Typically a bias voltage of +200 to +400 mV is used when bias cooling, although it is device dependent and can be varied between individual gates. With the bias cooling voltage applied, the sample can now be loaded as described in section 3.4.4.

When the sample has reached base temperature of ~20 mK, the first sensible test of the device is to measure the response of the Ohmic contacts (from hereon referred to as "ohmics"). For each ohmic, the I-V curve, current drawn as a function of

applied voltage, should be linear¹ and the resistance should be on the order of a few $k\Omega$ after accounting for the line resistance. Once the reliability of the ohmics have been established, one can then verify that the top gates are behaving as expected.

4.1.2 Quantum point contacts

Two ohmic contacts can be chosen; one, the *source*, has a voltage applied through eg. a DAC channel, and the other contact, the *drain* channel, is connected to ground via an Ithaco 1211 preamplifier as introduced in section 3.5.1, which measures the current being drained by outputting a proportional, measurable voltage.

In the absence of voltage being applied to the top gates, one then simply measures the current flowing through 2DEG between the Ohmic contacts (assuming the other ohmics on the device are electrically floating). In a top gate structure where two gates are separated by a short gap (sometimes called a "split gate"^[13]), a negative voltage can be applied to the gates to locally deplete the 2DEG underneath. This separates the 2DEG into two domains, connected by narrow channel through which the flow of electrons are constricted. This system is called a *quantum point contact* or **QPC**, illustrated in figure 4.1.

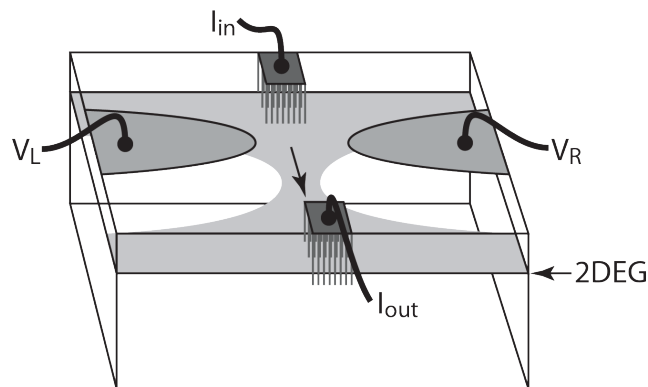


Figure 4.1: Schematic illustration of a quantum point contact, or QPC. V_L and V_R are the electric potentials of the left and right top gates constituting the QPC. I_{in} and I_{out} denote the current flowing through the source and drain ohmic respectively. Adapted from ref. [14]

The amount of constriction of the channel, and thus its conductance, can be controlled by varying the voltage on the top gates. At some point the current through the QPC is suppressed entirely, and in this case the gates are said to *pinch off* the 2DEG. Our devices are essentially more or less complex networks of QPCs intended to confine the 2DEG in controlled regions, and so the next logical step in testing a cooled device is to make sure that relevant pairs of gates pinch off successfully, by

¹ie. follow Ohms law, $I = U/R$, or the contact would not be very Ohmic!

verifying that the current between ohmics on either side of the QPC drops to zero at sufficiently negative gate bias.

The exact gate voltage at which this happens, the *pinch-off voltage*, provides an indicator for the effective width of the channel underneath. Ideally the pinch-off voltages should not be so high that gate leakage becomes a problem, and should be similar for gates with identical design. In the CB7 devices, the gates met in pairs, whereas in the NO7 devices the relevant pinch-off happened between a vertical gate and a horizontal "backbone" gate. In the latter case, the backbone gate was kept at a constant value and the pinch-off voltages of the individual gates could then be directly compared to each other.

In the limit of an electron channel confined to 1 dimension, there are only an integral amount of electronic modes that contribute to the electronic transport, with the result that the conduction is quantized in discrete levels of e^2/h . This effect can be observed in simple QPC systems^[14]. For our devices however, the length of the confined channel is on the same order as the Fermi wavelength in the 2DEG ($\lambda_F = \sqrt{\frac{2\pi}{n_S}} \approx 50 \text{ nm}$ [13]), so while quantum confinement does occasionally manifest itself as plateaus in the pinch-off curves, they are somewhat chaotic compared to longer channels. Nevertheless, it is useful to measure the conductance in units of e^2/h , the *universal quantum of conductance*, as it can be compared across devices and without regard for the applied bias voltage.

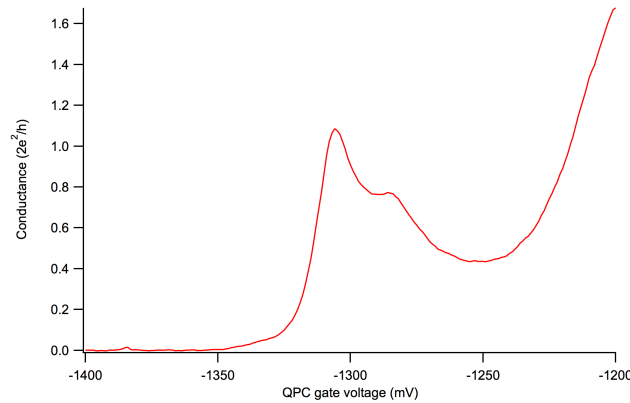


Figure 4.2: The conductance between the "QPC" gate versus left wall/plunger ("LW" and "LP") gates in a CB7 device. The pinch-off voltage of this gate is -1350 mV, subject to the voltages on the other gates: $V_{LW} = -600 \text{ mV}$. $V_{LP} = -550 \text{ mV}$.

4.1.3 Quantum dots

Having verified that individual gate pairs pinch off as they should, the next step is to check that quantum dots can be formed in the device as intended. Typically a quantum dot (QD, or simply "dot") is contained between two QPCs that define the tunnel barrier to the reservoirs of 2DEG or other quantum dots on either side. These are termed the "wall" gates, and are the ones primarily tuned to obtain the desired tunnel barrier, which should be at least on the order of a single resistance quantum ie. $>25k\Omega$. "Plunger" gates have the primary purpose of controlling the electrostatic potential of the dot. In all cases the gates affect the electronic environment broadly around them, so wall gates affect the electrostatic potential on the dot(s) and the plunger gates affect the tunnel coupling. This effect is called "cross coupling", and complicates tuning considerably as changing one parameter affects the others. Bias cooling, while beneficial for reducing noise in the device, exacerbates this effect as the footprint of a bias-cooled gate in the 2DEG increases^[14], causing higher cross capacitance.

To test a quantum dot, the 2DEG on either side of the dot is contacted as above, and the current through the dot is measured as the pair of QPCs confining the dot are pinched off. In the absence of quantum dot behaviour, one would expect the response to current to be suppressed if either QPC is below (more negative than) the pinchoff voltage, with some cross-coupling effect as one wall gate affects the pinch-off point of the other. If a quantum dot is successfully formed, one can observe current even

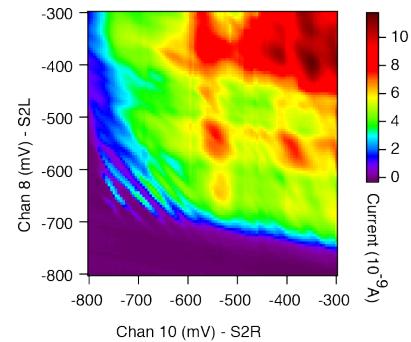


Figure 4.3: Wall/wall scan of a successfully formed quantum dot in NO7a.

below the expected mutual pinch-off voltages, on the condition that the chemical potential of a transition between two single-electron charge states in the dot falls within the source/drain bias window, giving rise to the characteristic Coulomb peaks in transport. Measuring the current through a dot as a function of the voltage on two confining wall gates is called a *wall/wall scan*, an example of which can be seen in figure 4.3, where a quantum dot was successfully formed in the Sensor 2 position of NO7a, see figure 4.6.

In the theoretical case where the wall gates only couple to the nearest tunnel barrier and not the opposite one, the conducting region in the wall/wall scan would be square, with the pinch-off curve of one QPC independent on the voltage of the other gate. In real systems however there is some measure of cross-coupling which causes the pinch-off lines to tilt at some angle. This angle can be used to quantify the degree of cross-coupling between gates. For example, in the wall/wall scan

shown in fig. 4.3, at $V_{S2R} = -300$ mV, the current is suppressed at $V_{S2L} \approx -755$ mV, whereas for $V_{S2R} = -500$ mV the corresponding pinch-off voltage is $V_{S2L} \approx -720$ mV. Changing V_{S2R} by 200 mV therefore corresponded to an equivalent V_{S2L} voltage of ≈ 35 mV, and the coupling factor of S2R on S2L is $\approx 18\%$ (regarding the pinch-off voltage at least). The coupling of one gate to the other is not necessarily equal to the coupling vice versa; for example in NO7a devices, the "horizontal" backbone gate (denoted "BB" for short) couples strongly to the tunnel barriers compared to the "vertical" wall gates.

The Coulomb peaks are visible as diagonal lines near the intersection of the pinch-off lines. The angle of the lines similarly betrays the coupling factor of the wall gates to the electronic energy levels in the QD. If the wall voltages are set somewhere in this region, the plunger gate which primarily couples to these energy levels can be swept in voltage, and the current will reveal the characteristic Coulomb peak structure of a quantum dot as seen in figure 4.4.

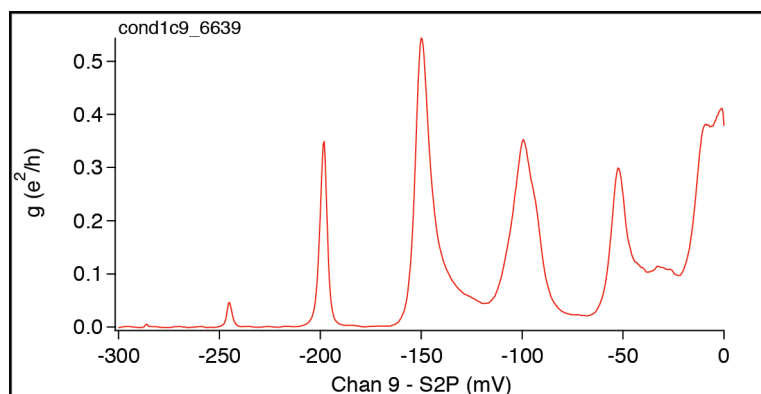


Figure 4.4: Coulomb peaks in S2 sensor quantum dot formed in NO7a, seen in fig. 4.3. Conductance through S2 is measured via SR830 Lock-in amplifier with applied voltage on sample $V_{app} = 20 \mu\text{V}$ at 37 Hz. Horizontal axis is the voltage on the S2P plunger gate. Other relevant gate voltages: $V_{S2L} = -555$ mV. $V_{S2R} = -565$ mV. $V_{BB} = -120$ mV.

4.2 Charge sensing

Measuring the DC transport of electrons through quantum dots is useful in performing diagnostics of one's device, as well as quickly homing in on a region of gate voltages where the device is configured roughly as intended. However, one is subject to some limitations: The lowest current practically measurable in the lab is on the order of a picoampere, corresponding to about 10^7 tunneling events per second. This necessitates fairly high tunnel couplings to either lead, which is unfavourable if one intends on using confined electrons to hold quantum information. One is also dependent on having leads on both sides of the structures being mea-

sured. To advance further, it is possible to use nearby quantum structures such as QPCs or sensor quantum dots (SQDs) for *charge sensing*.

Noting from the pinch-off curve shown in 4.2 that the conductance through QPC depends on the gate voltage, it is perhaps not a significant stretch of the imagination to visualize how the current is also sensitive to the local electrostatic environment. If one adjusts the gate voltage to a point on the pinch-off profile where the slope of the conductance is high, eg. around -1320 mV on the QPC gate in figure 4.2, the addition of a single electron to a nearby quantum dot causes a higher effective field the QPC channel resulting in a measurable change in the conductance. The technique was demonstrated by Sprinzak *et al.*^[25] to demonstrate detection of the charge states of a single quantum dot in 2002, and used later by Elzerman *et al.*^[9] to measure the charge occupation on two coupled quantum dots, ie. a double quantum dot (DQD) system. See figure 4.5 for a charge stability diagram of a DQD system in a CB7 device obtained via charge sensing using a QPC.

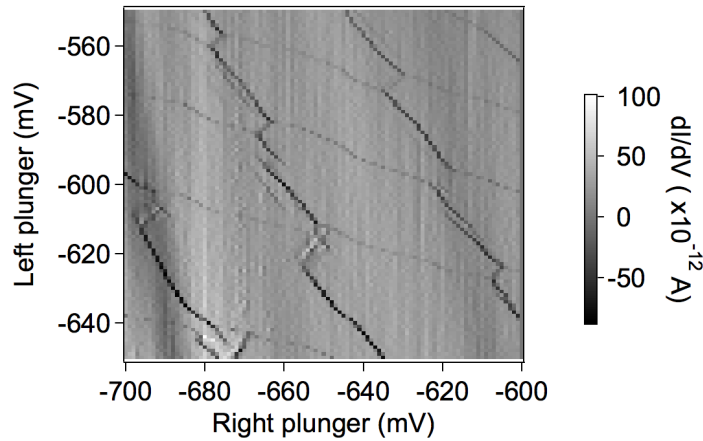


Figure 4.5: Charge sensing of double quantum dot "honeycomb" charge stability diagram in CB7 device using a QPC. The current was measured while sweeping the plunger gates of the DQD, and the derivative of the current is plotted in the graph to accentuate the changes in conductance between different charge states.

The sensitivity of a charge sensor depends on the slope of conductance versus gate voltage, $\frac{\delta g}{\delta V_g}$. The steeper the slope, the higher the change in the conductance from an additional nearby charge, and the higher the signal-to-noise ratio (SNR) becomes. Comparing the conductance curves in figures 4.2 and 4.4, it is then perhaps not surprising that using a quantum dot as a charge sensor offers increased sensitivity, as a quantum dot at a Coulomb peak is very sensitive to a change in voltage.

In the CB7 devices, a sensor quantum dot was designed on the right side of the DQD, although the success in forming quantum dots in this position has varied between individual devices. Barthel reports an increase in SNR of a factor 3 using

this SQD structure compared to using a QPC in a CB7 device^[3], although this is very specific to the device as well as the experimental setup.

There is usually a tradeoff in using a quantum dot for charge sensing in that the Coulomb peak is also very narrow, and therefore is only sensitive in a very narrow range outside which the conductance is suppressed due to Coulomb blockade. For this reason it is sometimes useful to use a QPC for charge sensing, as the conductance slope is wider and thus effective across a larger range in voltage.

As shown seen in the fig. 3.4 (p. 14), the NO7 devices were designed with five sensor quantum dots. Highly sensitive charge sensing was achieved using these with the NO7a device, an example being shown in figure 4.6.

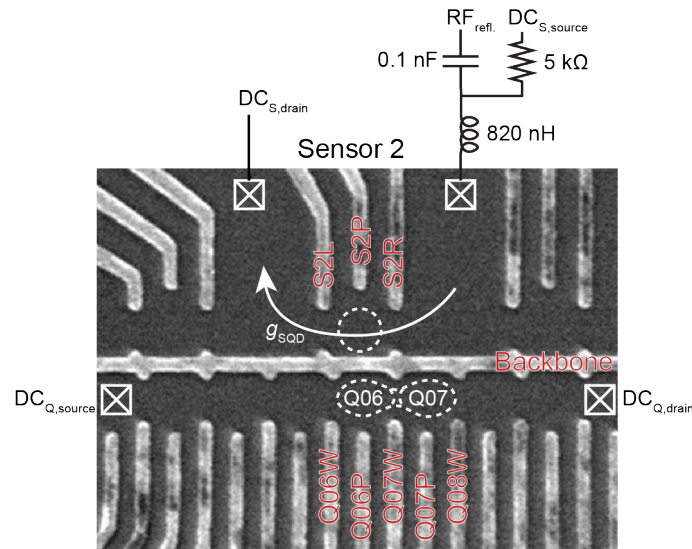


Figure 4.6: Charge sensing in NO7a device. The "S2" sensor quantum dot is used for charge sensing of a DQD in positions Q06/Q07.

The sensor quantum dot is defined by the wall gates S2L and S2R, which pinch off against the *backbone* gate. S2P is the *sensor plunger gate*. The confinement of the SQD has been described in section 4.1.3.

A double quantum dot (DQD) was defined in positions Q06 and Q07. The top gates Q06P and Q07P are the *plunger gates* primarily used to control the charge occupation of the dots. Gates Q06W, Q07W and Q08W are referred to as *wall gates*, the outermost being the primary control knobs of the coupling to the 2DEG leads on either side. Q07W is the "middle wall", and is the predominant influence on the interdot coupling. The walls also couple strongly to the potential of the dots. This causes the double dots to be highly dynamic systems, and changing the gates on the qubit-side ("south" of the backbone gate) also has a significant influence on the sensor dot which limits the effective range of the sensor dot with respect to sweeping gate voltages. However, the effect can be alleviated by adjusting the

voltage on the plunger gate of the sensor with the technique of *linear compensation* discussed further in section 5.1.

Information about the DQD can be obtained by measuring the dc transport current through the dots, by applying a voltage bias V_{SD} across $DC_{Q,source}$ and $DC_{Q,drain}$, the *source/drain bias*. However, this method fails as the quantum dots are strongly confined, increasing the tunnel barriers and suppressing the electron tunneling. A charge sensor, however, detects the electrostatic environment remotely, and can give information about the charge occupation on the dot where dc transport fails. A comparison between the two methods is shown in figure 4.7.

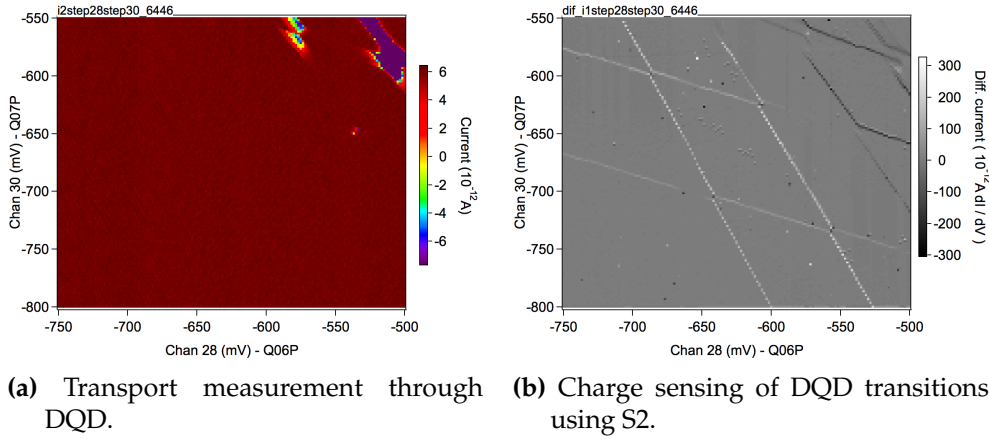


Figure 4.7: Comparison of dc transport across the DQD in positions Q06/Q07 on NO7a. The signal in (b) is the current through the S2 charge sensor, differentiated vertically to accentuate charge transitions. The charge stability diagram of the DQD can be resolved through charge sensing even to complete depletion, corresponding to the region in the lower left of 4.7b. The effective area of the charge sensor has been expanded through linear compensation of S2P, explained in section 5.1.

The compensated charge sensor reveals the charge stability diagram of the double dot, even down to complete electron depletion. A line in the charge stability diagram marks the transition between N and $N+1$ electrons populating the dot in the ground state, referred to as a *transition line*. The (mostly) vertical lines correspond to charge transitions in the Q06P dot, and the horizontal lines indicate charge transitions in Q07P. Exactly at a transition line the two charge configurations are degenerate, and at the triple points in the diagram electrons are able to tunnel through both dots coherently, resulting in "islands" of current in DC transport. To operate an electron spin qubit, the DQD is configured to be near a such charge transition.

Shown in figure 4.8 is the conductance of the S2 charge sensor measured by an SR830 Lock-in amplifier, used to measure a single charge transition of the DQD indicated in 4.6, although at a different tuning than in fig. 4.7. The diagonal line marks the transition between three electrons in Q06 and one electron in Q07 (blue region), versus two electrons in both dots (yellow region), also referred to as the (2,2)-(3,1) transition. The transition corresponds to the triple point at around (-540,-650) in fig. 4.7b.

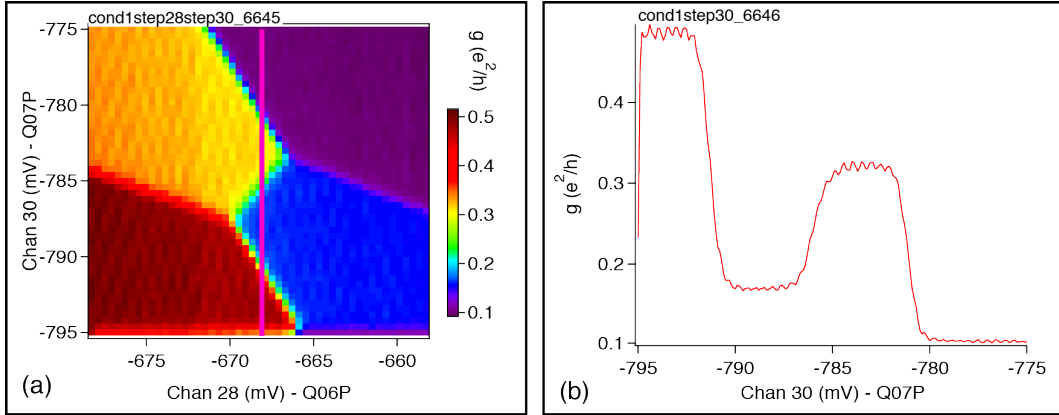


Figure 4.8: Charge sensing in NO7a using S2 sensor dot. Conductance through S2 is measured via SR830 Lock-in amplifier with applied voltage V_{app} : 20μ at 37 Hz. **(a)** Charge transition of a DQD in positions Q06 and Q07. **(b)** Conductance versus V_{Q07P} with $V_{\text{Q06P}} = -668.3$ mV, corresponding to the vertical line indicated in (a).

The four charge states are easily discerned as the sensor has been calibrated for highest sensitivity for this particular charge transition, but to measure another transition the sensor must be retuned. The sensor gates are configured as seen in fig. 4.4, with $V_{\text{S2P}} = -150.2$ mV, ie. the side of a Coulomb peak. Other features in the conductance sweep could be used in order to give sensitivity over a wider range, as used eg. in fig. 4.7(b). The periodic oscillations in the conductance measurement is probably due to the 37 Hz signal applied by the Lock-in amplifier, which could itself affect the charge sensor through capacitive coupling of the electric potential of the 2DEG. Nevertheless, the SNR is ~ 15 .

4.3 Reflectometry

So far, the charge sensing described has been done by measuring the current through a charge sensor, one way or the other, exclusively through the DC lines. This puts a limit on the bandwidth of measurements that can be performed due to the RC time constant of the lines, which specifically include RC filters to protect the device from high-frequency noise. Furthermore, electrical systems have ubiquitous $1/f$ noise (or "pink noise"), which sets a noise floor that necessitates time averaging. A single measurement using DC is on the timescale of tens of ms.

While this method can be useful for extracting ensemble averaged data on a qubit system, demonstrated by Petta *et al.* in 2005^[19], faster readout must be achieved if it is to be implemented in a functioning quantum computer. One method of accomplishing this is through reflectometry, which is the measurement of the reflection of AC signals from a junction of circuit elements with different impedances. This method was pioneered by Schoelkopf in 1998^[24], and implemented for solid state qubits by David Reilly in 2007^[22].

When a radio-frequency (RF) signal propagating in a transmission line with characteristic impedance Z_0 encounters a circuit element with impedance Z_L , some portion of the signal power is reflected at the junction. The ratio of the voltage of the reflected wave compared to the incident wave is defined as the *voltage reflection coefficient*, Γ , determined by the equation below^[21].

$$\Gamma = \frac{Z_L - Z_0}{Z_L + Z_0} \quad (4.1)$$

The reflection coefficient is thus sensitive to changes in the load impedance. If the source and load impedances are equal, the entire signal power is transmitted into the load, whereas significantly differing impedances result in high reflection. If a charge sensor is implemented as part of a resonant circuit, for example as the resistive element, and if the resonant circuit has an impedance very close to the characteristic impedance of the transmission line so that $\Gamma \approx 0$, a small change in the resistance (for example due to the tunneling of a nearby electron) will manifest as a significant change in the signal power reflected from the junction. Using high-frequency RF signals it is possible to achieve sufficiently high bandwidth and low noise to enable *single-shot readout*, the resolution of a single tunneling event in real-time. To use a qubit for efficient quantum computing it is necessary to measure the state of the qubit with high fidelity and on fast timescales, and single-shot readout using reflectometry is currently the best bet for qubits in solid state systems.

4.3.1 Impedance matching

To use reflectometry for readout of a charge sensor, the first requirement is that the resonant circuit in which the charge sensor is embedded has, at some frequency, an impedance close to the characteristic impedance of the transmission line, $Z_0 = 50\Omega$. If this condition is fulfilled, the circuit is said to be *impedance matched*.

As described in section 3.3, the reflectometry circuit in the experiment includes four parallel resonant RLC (or "tank") circuits, theoretically enabling fast sensing of multiple charge sensors simultaneously. The inductance L is determined by the surface-mount inductor coil soldered onto the Mayo board for each tank circuit, C is from the parasitic capacitance in the circuit experimentally determined to be around 0.9 pF, and R is dominated by the resistance of the charge sensor. For a conductance of $g \approx 0.5$, this corresponds to a resistance $R = 2R_K \approx 50\text{k}\Omega$.

The impedance of a circuit depends on the frequency ω of the applied AC signal. For a given electrical circuit, the input impedance Z of the circuit can be calculated from the impedances of the elements it consists of, calculated similarly to the equivalent resistance of a circuit of resistors in series and parallel. The tank circuits on the Mayo board each consist of an inductor ($Z_L = i\omega L$) in series with the resistance of the charge sensor ($Z_R = R$) parallel with the parasitic capacitance C_p of the inductor, bond wires etc. to ground ($Z_C = -i/\omega C_p$). The frequency-dependent impedance of the tank circuits are thus:

$$Z_{\text{tank}} = i\omega L + \frac{1}{\frac{1}{R} - \frac{\omega C_p}{i}} = i\omega L + \frac{1}{\frac{1}{R} + i\omega C_p} \quad (4.2)$$

For most frequencies, the impedance is prohibitively high. However, RLC circuits have the property that at a characteristic angular frequency ω_0 , the reactances of the inductors and capacitors cancel exactly, given by $\omega_0 = \frac{1}{\sqrt{LC}}$. This corresponds to a resonant frequency f_0 of:

$$f_0 = \frac{\omega_0}{2\pi} = \frac{1}{2\pi\sqrt{LC}} \quad (4.3)$$

The challenge of impedance matching a charge sensor is then that the input impedance is approximately 50Ω at the resonant frequency f_0 , simultaneously with matching resistance R being in a region where the charge sensor is sensitive. If R is too low or too high, a single charge will change the impedance of the sensing circuit negligibly. An example of successful impedance matching for $g \sim 0.5e^2/h$ can be seen in fig. 4.9.

A notable feature of fig. 4.9 is that the impedance matching is not purely dependent on the resistance ($R = R_K/g$), or matching would also be observed in the valley at lower QPC gate voltages where the conductance is also $0.55 e^2/h$. A pos-

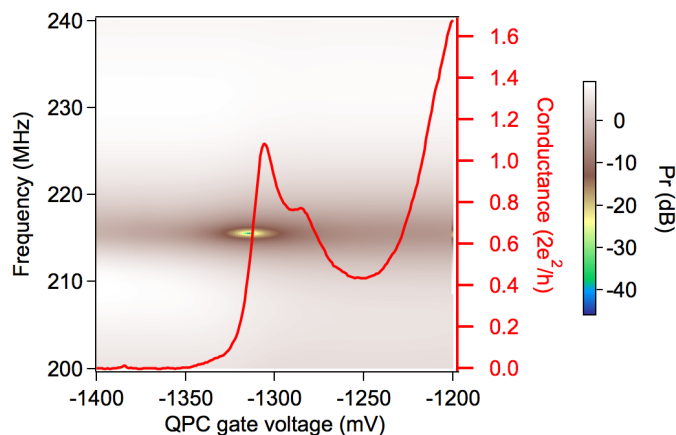


Figure 4.9: Impedance matching in CB7 3_4. Red trace: Conductance through QPC gate and left wall / plunger gates measured via SR830 Lock-in amplifier, identical with fig. 4.2. The color scale denotes reflected power as measured with a HP8753D network analyzer. Matching is observed at ~ 215 MHz, at a QPC conductance of $\sim 0.55 e^2/h$, where the reflected signal is attenuated ~ -45 dB, ie. nearly full power transmission into the tank circuit.

sible explanation is that the gate voltage also influences the capacitance of the tank circuit. All in all, impedance matching a charge sensing circuit is not a trivial task, and several attempts were not as succesful as the one pictured here.

4.3.2 Demodulation

With a suitably impedance-matched device, the next challenge that arises is to digitize the magnitude of the signal reflected from the interface between transmission line and tank circuit. This is achieved with the demodulation circuit, schematically illustrated in figure 3.12 (p. 29). The main principle involved is *homodyne detection*, which can be considered a special case of *heterodyne* (lit. "two-tone") detection, where the two tones are identical.

An important component in RF electronics is the *frequency mixer*. It is a nonlinear electrical circuit in which the output is the effectively the result of two applied signals being multiplied. Considering the instantaneous voltages V_1, V_2 of two alternating current (AC) signals with amplitudes A, B and frequencies f_1 and f_2 :

$$V_1 = A \sin(2\pi f_1 t) \quad (4.4)$$

$$V_2 = B \sin(2\pi f_2 t) \quad (4.5)$$

If the two waveforms are multiplied, one can use the trigonometric identity:

$$\sin(a) \cdot \sin(b) = \frac{1}{2} (\cos(a - b) - \cos(a + b)) \quad (4.6)$$

to derive:

$$V_1 \cdot V_2 = \frac{AB}{2} (\cos(2\pi(f_1 - f_2)t) - \cos(2\pi(f_1 + f_2)t)) \quad (4.7)$$

One observes that the multiplied waveform has components at the *sum* and *difference* of the input signal frequencies, $f_1 - f_2$ and $f_1 + f_2$. Multiplying a 10 kHz sine wave with a 11 kHz sine wave, the result would be a superposition of a 1 kHz wave (the "beat frequency"²) and a 21 kHz wave. If the signals are of the same frequency, the result is a $2f$ component with a certain DC offset. Low-pass filter the $2f$ component away, and you have a measurable DC signal that directly depends on the amplitudes of the input signals A and B . This is the principle of homodyne detection.

In the above calculation the signals were assumed to be in phase. In reality, there is a phase offset which should not be neglected. If the signals are out of phase, the DC component is suppressed. For this reason, the demodulation circuit includes a phase shifter, which can be adjusted to maximize the demodulated signal.

The frequency mixer used in the demodulation circuit, a Mini-Circuits ZP-3MH-S+, is a *double balanced mixer* relying on diodes to multiply two signals (see circuit diagram in fig. 4.10). The input ports are **L**, the *local oscillator*; **R**, the RF input, and the output port is the *intermediate frequency* or IF port, on the Mini-Circuits mixer denoted by an **X**.

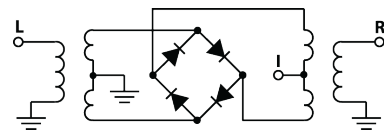
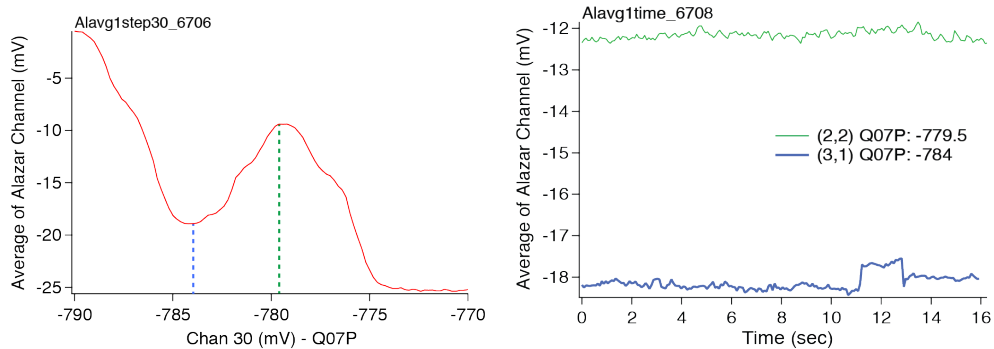


Figure 4.10: Circuit diagram of a double-balanced mixer.

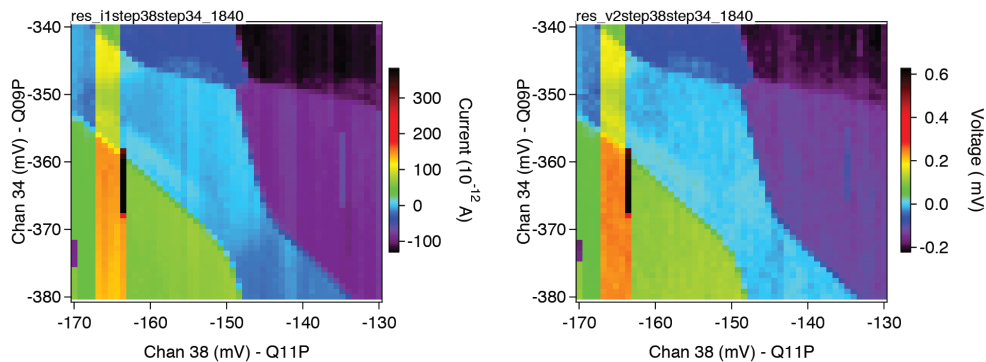
As already described in section 3.5.3, the reflectometry is achieved by generating a *carrier signal*, of which the predominant fraction of signal power is fed into the LO port of the mixer. A portion of the signal amplitude is sent to the sample via a directional coupler and various attenuators, and a portion is reflected proportional to the impedance mismatch as per eq. 4.1. The reflected signal is amplified and bandpass filtered, and finally sent into the RF port of the mixer. The IF output is low-pass filtered, and the DC component can be measured via a digital multimeter (DMM). An example of reflectometry readout of the S2 charge sensor can be seen in fig. 4.11.

²Musicians, like experimental physicists, use beat frequencies to tune their devices. If eg. two guitar strings aren't properly tuned, the result is a characteristic, undulating beating sound. Turn the knob until the beat frequency is inaudible; then you can reasonably claim that $f_1 \approx f_2$.



- (a) The demodulated reflectometry signal measured with the Alazar scope used in DMM mode as V_{Q07P} is swept through the (2,2)-(3,1) charge transition of a DQD. Compare fig. 4.8(a).
- (b) Demodulated signal measured over time for the (2,2) and (3,1) charge states, with V_{Q07P} situated at the valley and peak, respectively, indicated in (a).

Figure 4.11: Charge sensing with reflectometry in NO7a using S2 sensor dot. The device tuning is identical to that in fig. 4.8, in which the conductance through the SQD is measured with a lock-in. Each data point is averaged over 80 ms. The signal-to-noise ratio is ~ 41 for this integration time.



- (a) DC transport through sensor 4.
- (b) Demodulated reflectometry output measured via DMM.

Figure 4.12: Simultaneous charge sensing of a triple-dot formed in positions Q09/Q10/Q11 on NO7a using Sensor 4 SQD. Graphs have been corrected using `planefit()`, resulting in a "flatter" image. DC transport measurement in (a) shows slightly sharper transition lines, but the demodulated reflectometry signal in (b) has the potential to be read on very fast timescales. The vertical "bar" in both graphs correspond to a temporary device switch.

4.3.3 Fast readout

With a working charge sensor embedded in an impedance-matched tank circuit, the time is nearly ripe for taking lots of data. The demodulated reflectometry output is connected to an input on a fast digitizer, in our case the Alazar ATS9440 digital oscilloscope described in section 3.5.4. This enables fast readout with a theoretical maximum bandwidth of 65 MHz due to the specifications of the Alazar card.

However, it does not enable fast *control* of the device, since so far we are still controlling gate voltages via the DC lines. To progress, certain gates must be connected to the *fast lines*, described in section 3.5.2. On the wire bonding level, this involves bonding the intended *fast gates* to the fast gate pads on the Mayo board. Each fast gate pad is connected to a *bias tee*, a simple electrical circuit that combines an RF and DC signal. The RF input is routed to an SMP connector, which connects via a semi-rigid copper coax cable to a coax line in the cryostat (see figure 3.7 on p. 18). This enables high-frequency electrical signals to be sent from the SMA connectors on top of the cryostat to the device gate, through -25 or -28 dB attenuation depending on the coax line.

To leverage the power of the oscilloscope, the fast plunger gates are ramped with a saw-tooth waveform generated by HP33250A function generators. During this experiment we used one ramp, but in theory two plunger gates could be ramped simultaneously; one fast and one slow. The fastest readout that we managed to have working reliably was 951 Hz sawtooth ramping, ie. about 1 ms per ramp.

When starting a ramp, the HP33250A sent a synchronization signal which was used to trigger the Alazar card. When a trigger was received, it sampled a number of points of the demodulated reflectometry signal corresponding to the length of the ramp. Depending on the acquisition mode, a number of ramps were then collected and averaged over to yield the final trace, which was then sent to Igor via the PCI-Express interface. The "slow" plunger gate is then adjusted, and the cycle repeats until the charge sensing signal for the full 2D sweep has been acquired. The end result is a speed-up of nearly two orders of magnitude. An example of a sweep can be seen in fig. 4.13.

When acquiring fast traces, the size of the sweep window for the fast gate is limited by the maximum voltage that the HP33250 can output, ie. ± 2 V. Due to attenuation of the fast line there is a division factor that must be calibrated, which in our experiment was 35.3, to ensure that the dimensions of the acquired Alazar trace matches the actual voltage on the gate. With the division factor, the widest range in voltage that can be swept on the fast gate is ~ 55 mV, whereas the purely DC-controlled plunger gate can be swept across the entire voltage range of interest.

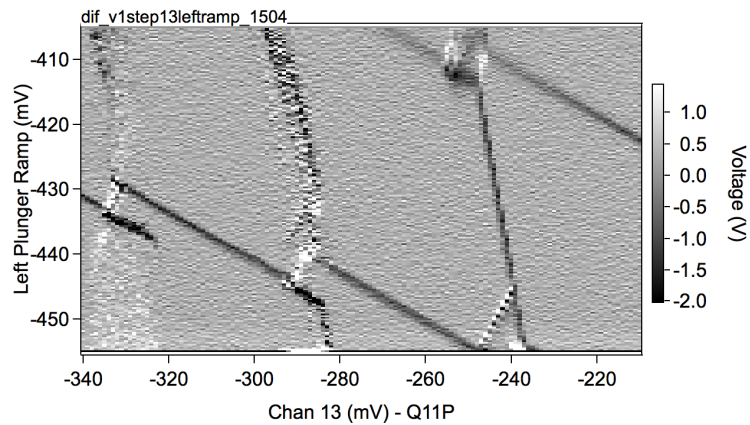


Figure 4.13: A charge stability sweep obtained using fast reflectometry readout as described in the text. The device is an attempted asymmetric double quantum dot formed in positions Q09+Q10/Q11 in NO7a. Gate Q09P was ramped by a HP33250 function generator at 951 Hz. 64 records were averaged per vertical trace. Q11P was swept in 131 steps. Acquisition time: 0.519 min.

This can be circumvented by taking a scan, offsetting the fast gate DC bias, taking another sweep, etc. and subsequently "stitching" each scan together in a bigger graph. This can be done by using the function `ConcatenateImages()`. An example of concatenated fast sweeps is shown in fig. 4.14.

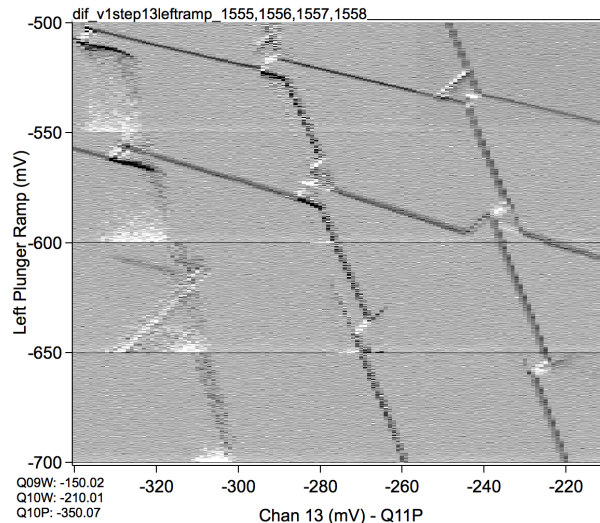


Figure 4.14: Fast reflectometry readout sweeps concatenated to a bigger graph. The device is the same as in fig. 4.13. The horizontal lines are due to artifacts in reflectometry.

5

Igor routines

During the Master's project several customized Igor functions have been developed and implemented to facilitate the experiments in various ways. While not necessarily breathtaking feats of computer science of interest to academia in general, they are perhaps useful for others in the lab, either for inspiration or direct implementation, and in this chapter I will briefly describe some of the notable contributions. The Igor procedure file containing the custom functions is uploaded on the QDev wiki¹.

5.1 Charge sensor compensation

When doing charge sensing measurements with a sensor quantum dot (SQD), one finds the sensor is only sensitive in a certain effective voltage range. When sweeping nearby gates, eg. the plunger gates of a double dot structure of interest, this manifests in the sensor losing sensitivity when the gates are swept too far from the equilibrium at which the sensor was calibrated. As tuning a DQD often involves scanning wide ranges in gate voltage, it is useful to alleviate this by linear compensation of the sensor plunger gate voltage, which can extend the operational range of the charge sensor.

The method relies on calculating the voltage that the sensor plunger must be offset by, ΔV_p , to counteract the effect of the contributions of the other gates being swept. First, with the device gates centered at the voltages of interest, defined $V_{\text{center},i}$, the sensor is tuned for optimal sensitivity and the wave center_voltages is defined:

$$\text{center_voltages} = \sum_i V_{\text{center},i} \quad (5.1)$$

¹File:Triton7procs.ipf (requires log-in)

This is implemented in the `CenterSensor()` function in Igor, which simply copies the DAC wave to `center_voltages` when the gates are centered. The old `center_voltages` wave is saved in `center_backup`, in case the centering should be reverted to the previous values.

```
function CenterSensor()
    wave DAC
    wave center_voltages
    duplicate/0 center_voltages center_backup
    duplicate/0 DAC center_voltages
end
```

For compensation to work, the coupling strength of each gate to the sensor dot must be known, normalized to that of the sensor plunger. Ie. changing the bias on a gate by 100 mV might require the sensor plunger to be offset by -12 mV, meaning a coupling strength of 0.12. Gates closer to the charge sensor have a higher coupling strength. The coupling strength α_i of gate i for each gate is saved in a wave, with separate waves for each sensor to allow easy switching between sensors being used. If sensor 2 is used, the relevant wave name is `S2couplings`:

$$\text{S2couplings} = \sum_i \alpha_i \quad (5.2)$$

There are several ways of obtaining the coupling strengths between a gate and the charge sensor, described in section 5.1.1. For now, we will assume that the coupling strengths have been measured, and the plunger gate offset ΔV_P can be calculated. The voltage difference of each gate from its center value is multiplied by the its coupling to the sensor, and the total contributions are summed to provide the total offset.

$$\Delta V_P = \sum_i \alpha_i (V_i - V_{\text{center},i}) \quad (5.3)$$

This is calculated in the function `adjustplunger()`, which also applies the calculated offset to the defined center voltage for the plunger. Calling `adjustplunger()` should therefore result in the used SQD being linearly adjusted for the current gate voltages.

```
function adjustplunger()
    variable index, setvoltage
    wave center_voltages, DAC
    NVAR plunger
    SVAR SensorStr
    wave couplings = $SensorStr
```

```

setvoltage = center_voltages[plunger] // base value

for(index=21;index<=39;index+=1) // if gates are on chans 21-39
    setvoltage += (center_voltages[index] - DAC[index])*couplings[index]
endfor
chanramp(plunger,setvoltage) // ramps plunger gate voltage
end

```

This functionality is integrated in the `setval()` routine described in section 3.6.1 for a customized `idstr`. For doing a compensated 2D sweep of gate voltages, the outer sweeping loop (the "stepper") sets a gate voltage and calls `adjustplunger()`. The subroutine has the identifier string "step<#>", where <#> is the number of the DAC channel being updated, similar to the "c<#>" `idstr`.

```

function setval(idstr,value)
    string idstr
    variable value
    [...]
    elseif(stringmatch(idstr[0,3], "step"))
        num = str2num(idstr[4,5])
        chanramp(num,value)
        adjustplunger()
    [...]
end

```

5.1.1 Calibration of SQD coupling strengths

The coupling strength α_i of gate i to a charge sensor can be found in several ways. One is to offset the gate by a certain voltage and observe the shift of the conductance features as the sensor gate is swept. For example, if a gate voltage V_g is offset by 20 mV and a Coulomb peak of the SQD is shifted by -4 mV in sensor plunger gate voltage V_p , the coupling $\alpha_g = -\frac{4}{20} = 0.2$. This process is automated in the `measureCoupling()` function:

```

function measureCoupling(chan,voltage[,stopchan])
    variable chan, voltage, stopchan
    wave DAC

    variable Vmax1, Vmax2, offset, width
    NVAR plunger
    SVAR SensorStr

    wave couplings = $SensorStr

```

```

if( ParamIsDefault(stopchan))
    stopchan = chan
endif

offset = 20 // value to displace gate voltage in mV
width = 20 // range in mV around voltage to scan for peak

// first: Acquire base peak
chanramp(plunger,voltage+width/2) ; wait(0.2)
do1d("c"+num2str(plunger),voltage+width/2,voltage-width/2,400,0.01)
wavestats/Q $toptrace(0)
findpeak/Q/M=(V_max*0.75)/B=9 $toptrace(0)
Vmax1 = V_PeakLoc
TextBox/C/N=text0/F=0/A=LT "Calibrating offset\rBase trace\rPeak: "
    +num2str(Vmax1)

// now offset each channel, retake trace, compare peaks and update
// offset value
for(chan=chan;chan<=stopchan;chan+=1)
    chanramp(chan,DAC[chan]-offset)
    chanramp(plunger,voltage+width/2) ; wait(0.2)
    do1d("c"+num2str(plunger),voltage+width/2,voltage-width/2,400,0.01)
    chanramp(chan,DAC[chan]+offset)
    wavestats/Q $toptrace(0)
    findpeak/Q/M=(V_max*0.75)/B=5 $toptrace(0)
    Vmax2 = V_PeakLoc
    couplings[chan] = (Vmax2 - Vmax1)/offset
    TextBox/C/N=text0/F=0/A=LT "Calibrating offset\rC"+num2str(chan)+
        " -"+num2str(offset)+" mV\rPeak: "+num2str(Vmax2)+
        "\rCoupling: "+num2str(couplings[chan])
endfor
end

```

The function assumes that stream 1 defined in the DataControl macro returns the conductance; that the global string SensorStr is the name of the wave with coupling strengths to the sensor being calibrated, eg. S2couplings; and that the global variable plunger is the number of the DAC channel controlling the sensor plunger. The voltage parameter is the plunger gate voltage at which the function looks for a Coulomb peak. If the optional stopchan parameter is declared, it will scan a range of DAC channels.

Thus, if one wants to measure the coupling strengths of the gates connected to the range of DAC channels 16 to 21, tracking the offset of a Coulomb peak at $V_P = -125$ mV, one calls the command: `measureCoupling(16,-125,stopchan=21)`. One then goes for a cup of coffee or a group meeting, returning to a set of commented plunger sweeps and an updated wave of coupling strengths.

It is useful to check the graphs for obvious mistakes, and some fine-tuning of the coupling strengths can also be done as the experiments proceed. Ideally, the offset applied to the gate being measured should not cause a change in the electron occupation of a nearby quantum dot, as it would cause the measured coupling strength to be inaccurate, although the function described above does not take this into account. Still, it is useful to obtain a ball-park value of the coupling for a range of channels.

A method of accurately determining a coupling strength of a gate is to iteratively run a 1D sweep of the gate voltage using the "step" idstr. For an accurate coupling strength, the conductance of SQD should be horizontal as the gate is swept, with plateaus indicating only electronic tunneling events. The coupling strength is manually adjusted between sweeps until this is achieved. The sensor can even be overcompensated, so that the change in electrostatic energy from electron tunneling is also compensated for, extending the effective range of the sensor even further.

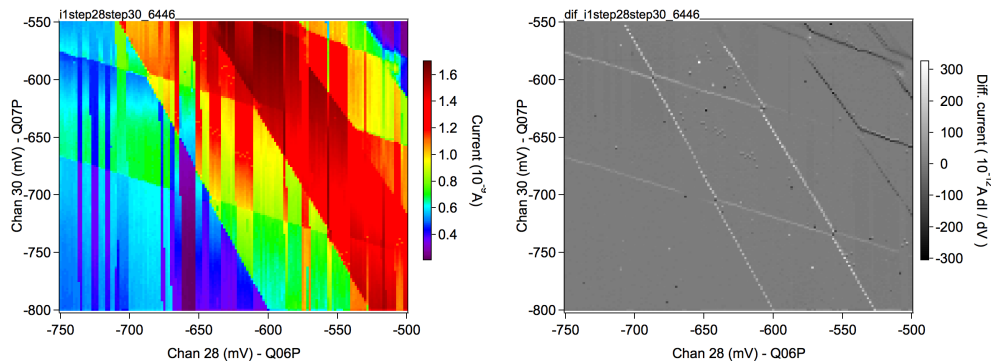


Figure 5.1: Charge sensing of a DQD on NO7a enabled through linear compensation of the sensor plunger gate. Left: Current through SQD measured via Ithaco. Right: The current of the left graph differentiated vertically. The region in the lower left of the graph is the complete depletion of electrons in the double dot.

5.2 Automatic charge sensor calibration

It is frequently the case that a charge sensor needs to be calibrated, ie. the sensor plunger gate voltage, V_P , adjusted so that the charge sensor is in a sensitive regime. To do this manually, the conductance through the SQD is measured as a function of V_P , also known as a *plunger sweep*, described in section 4.2 on page 43. A voltage is chosen such that $\frac{\delta g}{V_P}$ is high as well as consistently sloped over a reasonable range of voltage.

Depending on the stability of the device, there may be *switching* events, for example the population or depopulation of a charge donor in the semiconductor, which changes the electrostatic environment of the sensor dot. This causes loss of sensitivity. It may also simply be the case that gate voltages have been adjusted sufficiently for the charge dynamics to change. One then needs to recalibrate the sensor, but luckily this can be done semi-automatically.

The function `CalSensorCenter()` has been written for this purpose. Given a setpoint value of sensor conductance, it will adjust V_P in small increments while measuring the sensor conductance, eg. through the voltage output of the reflectometry circuit, until the setpoint is reached. The function integrates with `adjustPlunger()` described above to update the center voltage of the sensor plunger.

```
function CalSensorCenter(midpoint) //for charge sensing via sensor dot
    variable midpoint
    variable signal, startval, boundsflag
    NVAR plunger // DAC channel of sensor plunger gate
    wave center_voltages

    // user customizable values
    variable stepsize = 0.1
    variable maxdeviation = 25 // mV - to prevent ramping sensor forever

    boundsflag = 0

    adjustplunger()
    signal = getdata(1)
    startval = center_voltages[plunger]
    if(signal>midpoint)
        do
            center_voltages[plunger]-=stepsize
            adjustplunger()
            wait(0.01)
            signal = getdata(1)
            if(abs(center_voltages[plunger]-startval)>maxdeviation)
                boundsflag = 1
                break
```

```
        endif
        while(signal>midpoint)
    else
        do
        center_voltages[plunger]+=stepsize
        adjustplunger()
        wait(0.01)
        signal = getdata(1)
        if(abs(center_voltages[plunger]-startval)>maxdeviation)
            boundsflag = 1
            break
        endif
        while(signal<midpoint)
    endif

    if(boundsflag==0)
        print "Sensor calibrated! Start value: "+num2str(startval)+
            " end value: "+num2str(center_voltages[plunger])
    else
        printf "Calibration did not converge after varying %g mV.
            Resetting.\r",maxdeviation
        center_voltages[plunger] = startval
    endif
end
```

5.3 Automatic backup of DAC state of scans

A feature that proved very useful during experimentation, yet was comparatively easy to implement, was a function that saved the wave with DAC (ie. gate) voltages for future reference, and corresponding function that allowed one to quickly revert to this state, inspired by *saving* and *loading* as used in computer games.

The voltages output on the DACs are stored in the wave named "DAC". Simply, a copy of this wave was made after the creation of a new wave by a do1d or do2d scan. The function that copied the DAC wave is `SaveDAC(name)`, where *name* is a string with the name of the copied wave.

```
function SaveDAC(name)        // saves DAC wave to root:DACsaves:name
    string name
    wave DAC

    NewDataFolder/0 root:DACsaves
    name = "root:DACsaves:"+name
    duplicate DAC, $name
//    print "DAC voltages saved in wave:",name
end
```

After a `do1d()` or `do2d()` scan has been completed, the DAC wave is automatically saved in the Igor data folder `root:DACsaves`. This is done by integrating the following line of code near the end of the data taking loop:

```
SaveDAC("dac_"+num2str(nw))
```

where `nw` is the number of the wave used by the `do1d()` and `do2d()` functions. The saved wave can then be retrieved by entering a command like:

```
edit root:DACsaves:dac_123
```

which opens a table in Igor with the DAC voltages for wave number 123. If one is interested in a particular voltage, eg. on channel 15, it can be quickly retrieved by typing:

```
print root:DACsaves:dac_123[15]
```

If one wants to revert the experiment to an earlier state, this can be quickly done using `LoadDAC(name)`:

```
function LoadDAC(name) // loads wave saved with SaveDAC with setvals
    string name
    variable i
    name = "root:DACsaves:"+name
    wave dacvals = $name
    wave DAC

    for(i=0; i<numpnts(DAC); i+=1)
        if(DAC[i]!=dacvals[i])
            print "Setting channel "+num2str(i)+" to "+num2str(dacvals[i])
                +" from "+num2str(DAC[i])
            setval("c"+num2str(i),dacvals[i])
        endif
    endfor
end
```

Which simply runs a `setvals` for each element in the list if the DAC channel is not already at this value.

Logging of the DAC wave was also implemented by Alex Johnson in `logwave()`, which created an entry in a `.txt` log file, one for each day. While it was still possible to find the information on DAC voltages of a wave, it often involved searching through several log files. Saving the wave in the experiment file makes the information quickly retrievable, and the functions can furthermore be integrated in custom user functions, making it easier to set the experiment in a certain state rather than keeping track of gate voltages individually.

5.4 FeatureScan()

When tuning, it is sometimes the case that one is looking at a certain feature, such as a pair of bias triangles in a double dot transition, at a very specific set of gate voltages. If one wants to change a parameter, such as the interdot coupling or the coupling of a dot to a lead, the voltages of the gate confining the DQD is changed, which also has the side effect of changing the plunger gate voltages at which the feature appears in a 2D plunger sweep. This can be accounted for by sweeping a different window of bias voltages based on an estimate of how much the target has moved subject to the coupling strength of the varied gate relative to the plunger gates, or by sweeping a larger gate bias window at a cost of either resolution or time. Since tuning is an iterative process, the extra time quickly adds up, and therefore I wrote a function called `FeatureScan()`.

This function alleviates the problem by calculating the offset to the plunger gates due to the changed wall gate voltage, similar to how `adjustplunger()` calculates the plunger offset. The gate voltages are set to the center of the feature under investigation, and the voltages are saved in the `center_feature` wave by calling the function `CenterFeature()`.

The determine the offset, coupling strengths of the gates to the calibrated also, which are saved in the two-dimensional `couplings_feature` wave. Say you are taking scans by sweeping plunger gates on DAC channels 12 and 14. You adjust the gate on channel 19 by +10 mV, which causes the feature to shift -5 mV on c12, and +3 mV on c14. Update couplings like this:

```
couplings_feature[19][12] = -0.5
couplings_feature[19][14] = 0.3
```

To do a scan, call:

```
FeatureScan(channel1, channel2, width, steps [, s_label])
```

where `channel1` and `channel2` are integers, corresponding to the swept DAC channels (eg. 12 and 14). *Width*: the width of the scan window in mV. This also determines the height unless the aspect ratio is changed in the code from the default of 1:1. *Steps*: Amount of steps in each sweep. Same for both swept channels. *s_label*: If you want to label the graph window(s), do `s_label = "text"`.

FeatureScan enables high-resolution data acquisition of a particular feature without the need for manual adjustment between scans, making it useful for automated overnight routines for sweeping a wide range of parameters. An example usage could be:

```
function overnight()
    variable LWvoltage // voltage on left wall gate of DQD
    variable MWvoltage // voltage on middle wall gate of DQD

    for(LWvoltage = -175; LWvoltage <= -155; LWvoltage += 10)
        setval("c11",LWvoltage)

        for(MWvoltage = -110; MWvoltage <= -90; MWvoltage += 10)
            setval("c13",MWvoltage)
            FeatureScan(12,14,30,100,s_label="LW: "+num2str(LWvoltage)+
                " MW: "+num2str(MWvoltage))
        endfor
    endfor
end
```

This function will vary the voltage on the outer left wall and middle wall of the double dot, resulting in 3x3 high-resolution scans. This way, you can feel productive even while sleeping! A result from an overnight scan similar to the example is shown in figure 5.2. It is made visible how changing the wall voltages affects the electron tunneling dynamics through the DQD, manifesting in different structures of the bias triangles.

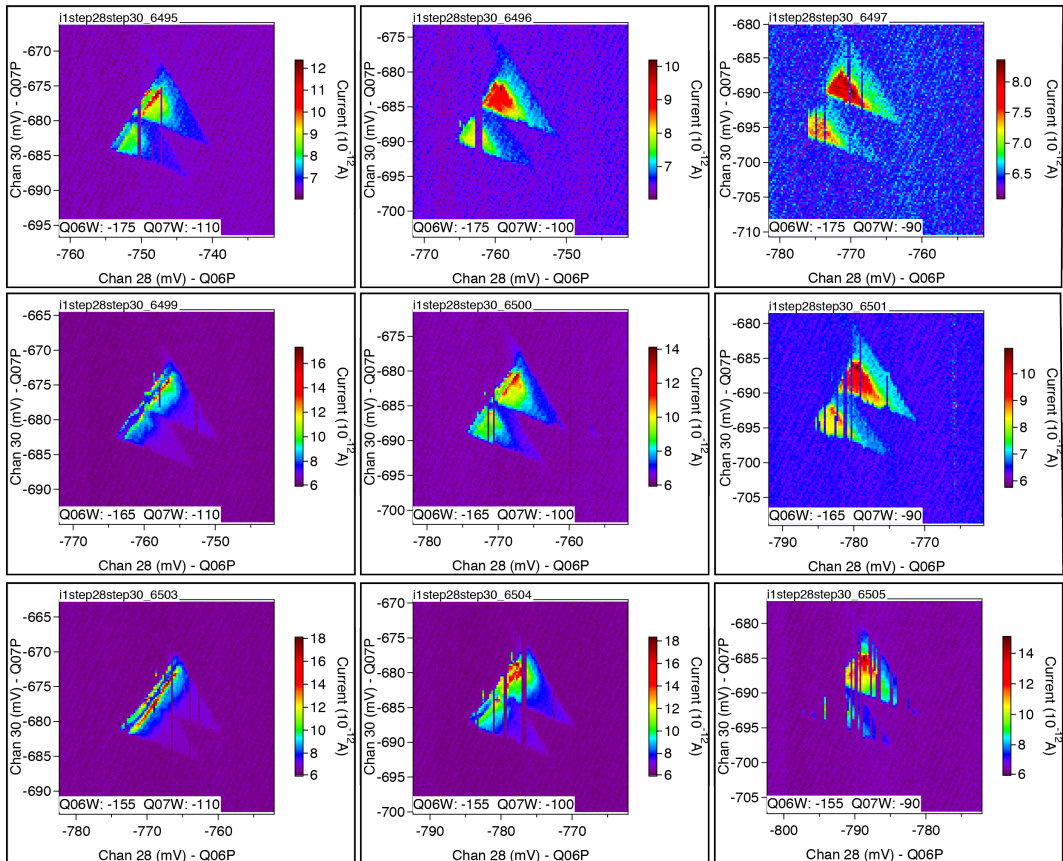


Figure 5.2: Bias triangles at (2,1)-(1,2) transition of DQD formed in NO7a at positions 6 and 7, with the left wall (Q06W) and middle wall (Q07W) varied. Scans were taken with FeatureScan() function, which adjusted the scan window to keep the bias triangles centered. As the wall gates are opened, the transition is pushed towards very negative plunger voltages which causes increasing instability.

6

Results

In this chapter I will present some of the experimental achievements and results that were reached during the project.

The first devices that we cooled down and measured were on the CB7 sample as reported on by Christian Barthel^[4] as well as Andrew Higginbotham and Ferdinand Kümmeth^[12]. Not all devices had survived the journey from Harvard, but we did manage to verify that our cryostat, equipment and minds were capable of bonding, cooling, tuning and measuring double quantum dot systems.

With the goal of fabricating a versatile work-horse device, in the optimal case with the potential of implementing no less than five qubits simultaneously, several generations of linear 15-dot devices were laboriously fabricated by Nastasia Okulova and Peter Dahl Nissen and tested. Some had faulty ohmics; some did not pinch off between gates as intended; for some, a previously solid fabrication technique had lost its reliability because of instrumentation issues. However, on the seventh generation we discovered a device that had made it through its entire fabrication run as intended.

On the third cooldown attempt we found a bias cooling voltage where the device was remarkably stable, and it was cold for a long time during which we were primarily tuning it towards holding up to three triple quantum dots simultaneously. An example of a characteristic "house" structure in the charge stability diagram of a successfully balanced triple dot can be seen in fig. 4.12 on page 52. After managing to tune at least two sets of triple dots independently but not simultaneously, we concluded that the linear dot structure of NO7a was not amenable for this application since the triple-dots had limited access to an electron reservoir when tuned in series. The next generation of devices accounting for this limitation is now in fabrication.

After the triple-dot hunt, it was my turn to proceed with my project of investigating the potential benefit in implementing a S-T₀ qubit on variations of the

standard DQD system. Some progress was made, as reflectometry readout was implemented and a Pauli spin blockade was demonstrated in a balanced double quantum dot. Full electron depletion was also accomplished, enabling unambiguous assignment of the electron occupancies in the charge regions observed. For an example, see fig. 5.1 on page 5.1.

During attempts to implement spin-to-charge conversion in the double dots tuned, the experiment was aborted due to what is known as a "fridge block". This is when the circulation of helium mixture in the dilution unit is impeded due to buildup of impurities. Thus, cooling fails and a full warm-up of the fridge is required, and the block must be cleared by turbopumping on the helium circuit in the cryostat to regenerate cold traps. We also took this chance to fix some hardware issues. Bent pins on the SMP connectors on the cold finger had meant that certain fast gates could not be functional, and while workarounds had been implemented it was short of the ideal of fully functioning cryostats.

With the sample warmed up, and since retuning is generally not a trivial matter, we took the chance to investigate some other samples in the NO7 series with different scaling factors. However, of devices NO7b and NO7f, neither device was functional and later investigation of the devices with Secondary Electron Microscopy revealed that the devices either did not come out of fabrication as intended, or possibly had been destroyed by static discharge during handling.

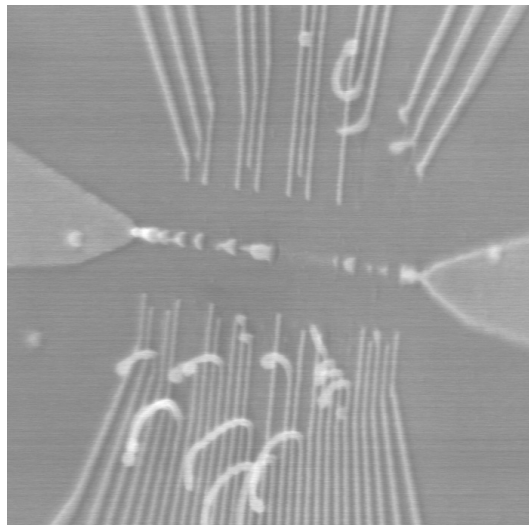


Figure 6.1: SEM micrograph of device NO7b tilted at an angle, at a magnification of 35,000x.

The intention was now to cool down device NO7a which, despite some imperfections, had been known to reliably confine quantum dots. However, a critical electrical error was discovered, and experiments had to be postponed until it was fixed. The fault was of that insidious variety which only manifests at cryogenic temperatures, and we spent several weeks doing fridge diagnostics. Another error, unrelated but equally critical in nature was located and alleviated in the process, in which the cryoamp of the reflectometry Rx line had developed an electrical leak to ground on its power cable. In the end, we managed to locate the problem to a faulty DC block. Replacing this experiments could continue, although the remaining timeframe was limited.

The purpose at this point was to attempt to implement asymmetric double quantum dots in NO7a, being double dot systems in which one dot was significantly bigger or more populated than the other, which could potentially have a beneficial effect on the system's properties as a qubit due to screening effects.

In the fourth cooldown of NO7a, it was found that the charge sensors had become somewhat unstable, evident in the charge sensing measurement shown in figure 6.2.

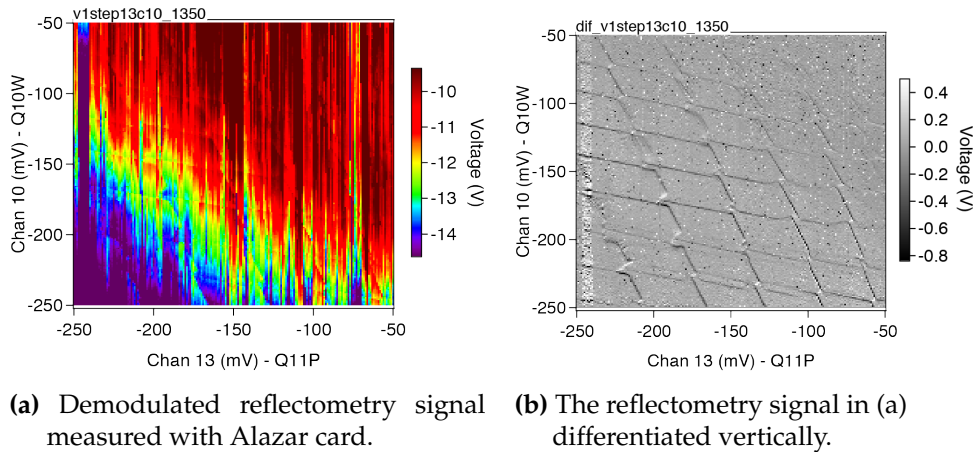


Figure 6.2: Charge measurement of an attempted asymmetric DQD in device NO7a with significant sensor switching. Differentiating the signal reveals the charge stability diagram. The sensor was compensated for the gate voltages swept to increase the effective range as described in section 5.1.

With the high level of switching in the sensor it was dubious whether the device could be used for any serious experiments. It could possibly have been alleviated by attempting another bias cooling, but the limited timeframe in mind I decided to make an attempt. By experimenting with the various control parameters I found some methods to reduce the sensor noise, by using gate voltages in certain ranges and applying a DC bias across the charge sensor, but it was still afflicted by frequent switches. The challenge was then to take the measurements on a faster timescale

than the noise. In this process I implemented fast reflectometry readout described in section 4.3.3 as well as the automatic sensor calibration described in section 5.2. This enabled me to obtain high-resolution charge sensing signatures of bias triangles at few-electron charge transitions.

6.1 Pauli spin blockade in NO7a DQD

Pauli spin blockade has been demonstrated, which is the suppression of current from e.g. a (1,1) charge state of a DQD into a (2,0) charge state due to Pauli exclusion of the electrons. This phenomenon is a prerequisite for high-frequency control of singlet-triplet qubits, and is thus a proof-of-concept for the validity of the NO7a device for use in implementing electron spin qubits.

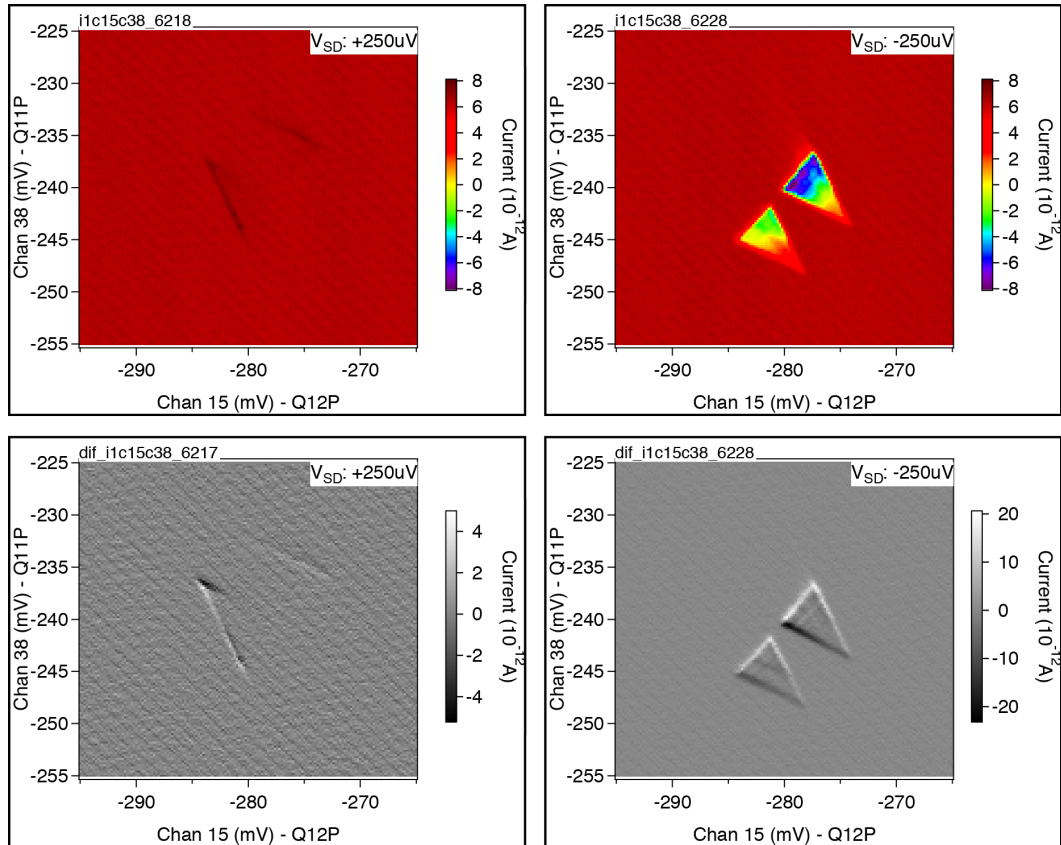


Figure 6.3: Pauli spin blockade demonstrated in Q11/Q12 DQD in device NO7a.

Top graphs: Transport through dots at positive and negative V_{SD} .

Bottom graphs: Data from top graphs differentiated vertically.

6.2 Fast readout via reflectometry

A reflectometry circuit was implemented as described in sections 3.5.3 and 4.3.3. To quantify its performance, traces were taken at three different charge states near a triple point of an asymmetric double quantum dot in positions Q09+10/Q11 in NO7a. The sensor used was S4. The charge states are indicated in figure 6.4. The difference in the blue and green traces correspond to the addition of an electron in Q11P, closest to the sensor, and the difference in green and red traces correspond to an extra electron in the big dot.

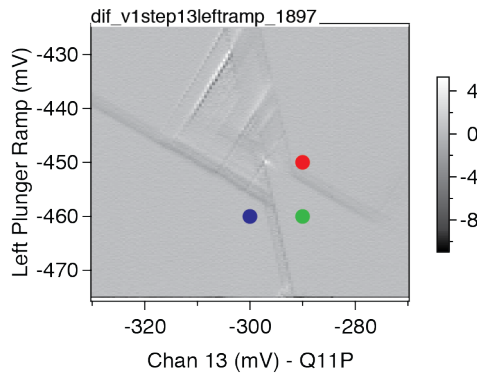


Figure 6.4: Charge transitions used to test the reflectometry performance via Alazar. The coloured dots correspond to the positions where the traces in fig. 6.5 were taken.

Figure 6.5 shows a subset of the full traces acquired, which consisted of 2^{14} (16384) pts at 100 MHz clock speed, corresponding to $\sim 164 \mu\text{s}$ of sampling. These traces are used to extract a noise spectrum, as well as a signal-to-noise ratio.

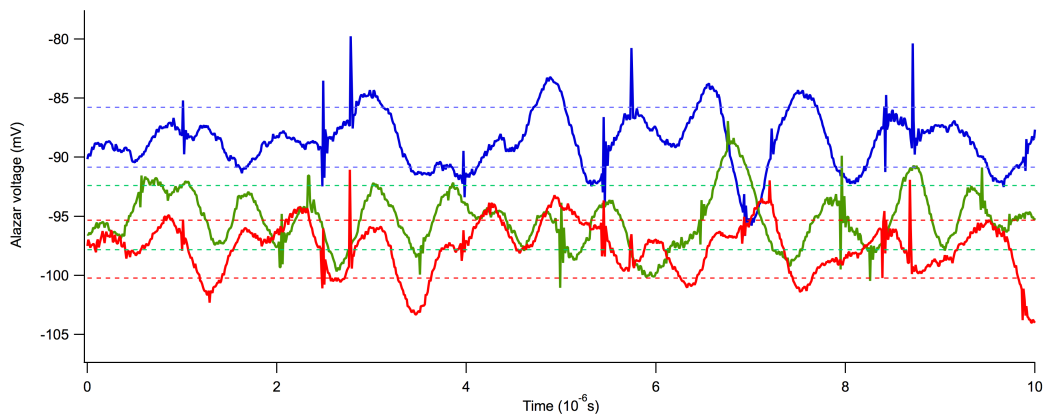


Figure 6.5: Raw demodulated voltage acquired by Alazar. A $10 \mu\text{s}$ subset of the total acquired trace is shown.

The average voltages for each wave are:

$$V_{\text{avg,red}} = -97.77 \text{ mV}$$

$$V_{\text{avg,green}} = -95.11 \text{ mV}$$

$$V_{\text{avg,blue}} = -88.31 \text{ mV}$$

With standard deviations of $\sigma_{\text{red}} = 1.97 \text{ mV}$; $\sigma_{\text{green}} = 2.18 \text{ mV}$ and $\sigma_{\text{blue}} = 2.02 \text{ mV}$ respectively. An average standard deviation of $\sigma_{\text{avg}} = 2.10 \text{ mV}$ will be used for SNR calculation.

For the full integration time, the signal-to-noise ratios for the electron additions are then:

$$\text{SNR}_{Q11} = \frac{V_{\text{avg,green}} - V_{\text{avg,blue}}}{\sigma_{\text{avg}}} = 3.24$$

$$\text{SNR}_{Q09+10} = \frac{V_{\text{avg,red}} - V_{\text{avg,green}}}{\sigma_{\text{avg}}} = 1.27$$

Although sufficient to distinguish charge states, these SNR figures are significantly less than one would hope if single-shot readout is the goal. The sensitivity is dependent on the particular stability and $\frac{dg}{dV}$ slope of the charge sensor, in this case S4, but the raw reflectometry data shown in fig. 6.5 looks somewhat self-correlated. The autocorrelation function of the red trace is shown in fig. 6.6.

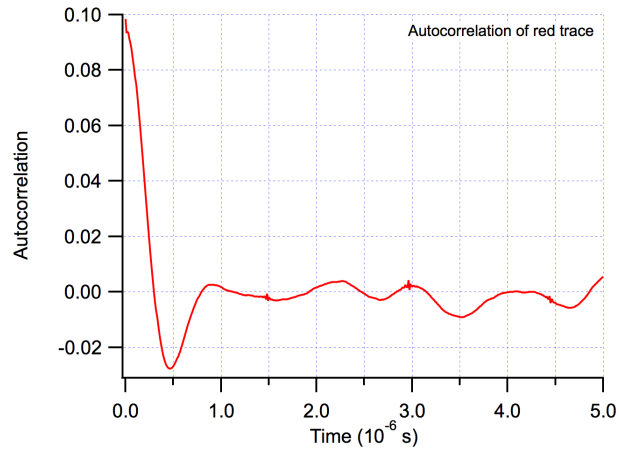


Figure 6.6: Autocorrelation of the raw reflectometry signal of the red trace in fig. 6.5.

The autocorrelation function reveals that the signal is self-correlated up to $0.9 \mu\text{s}$, corresponding to slightly above 1 MHz . This indicates that the bandwidth of the reflectometry circuit is set elsewhere, and that this signal is oversampled significantly by the Alazar card's bandwidth of 65 MHz .

Fourier transforms of the traces are shown in fig. 6.7, revealing a 3dB point , revealing an effective bandwidth of around 1.3 MHz .

Reviewing the components of the reflectometry circuit revealed that the SR560 Low-Noise amplifier, used to amplify the signal between the frequency mixer output and the Alazar input, is in all probability the culprit, as it has a nominal band-

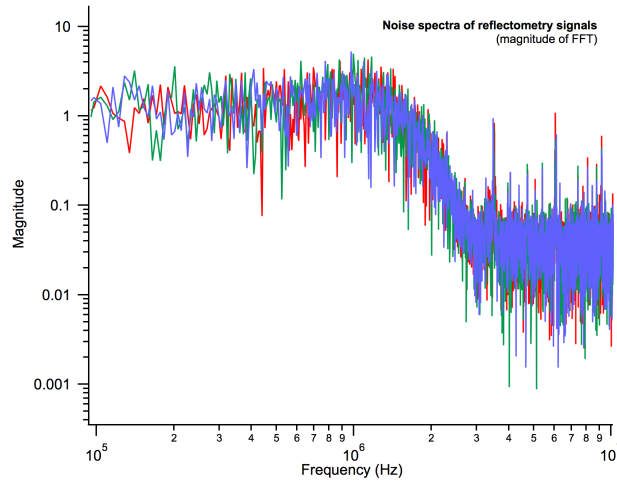


Figure 6.7: Fourier transform of the raw reflectometry signals in fig. 6.5.

width of 1 MHz. It should be an easy matter to remove this component from the reflectometry resulting in a marked increase of bandwidth.

6.3 Asymmetric double quantum dots

Having established the potential of the NO7a device for configuring double quantum dot structures, I attempted to configure an asymmetric DQD system where one of the quantum dots would be spread across two quantum dots as originally designed, seen in fig. 3.4. The positions chosen were Q09 and Q10 for the "big" dot, and Q11 for the "small" dot, located close to the S4 sensor quantum dot. As a first approach, the wall gate in-between Q09 and Q10 (gate Q10W) was set to a low voltage, and the Q09P and Q10P gates used simultaneously as plunger gates. It was observed that the big dot exhibited characteristics of two quantum dots - one coupling about equally to Q09P and Q10P, and one coupling most strongly to Q09P. In a sense an asymmetric double quantum dot was accomplished, but one of unknown and quite unreproducible origin.

Another tuning approach was attempted, in which the majority of the big dot would be in Q10, and the middle wall (Q10W) would be used for a plunger. This method also resulted in double dot behaviour, visible in the doubling of transition lines at negative Q10W voltages in figure 6.2. It proved difficult to configure a quantum dot spanning two positions as it was likely to break up at low gate voltages, however an attempt was made.

Fast reflectometry readout was employed to resolve the fine structure in the bias triangles around triple points in the charge stability diagram of the asymmetric DQD seen in fig. 6.2. It was not possible to determine the electron occupation

exactly, in part due to the unstable nature of the quantum dots meaning that the usual method of emptying the system completely and loading electrons one by one was not possible. An example of a bias triangle pair at positive and negative source/drain biases is shown in figure 6.8.

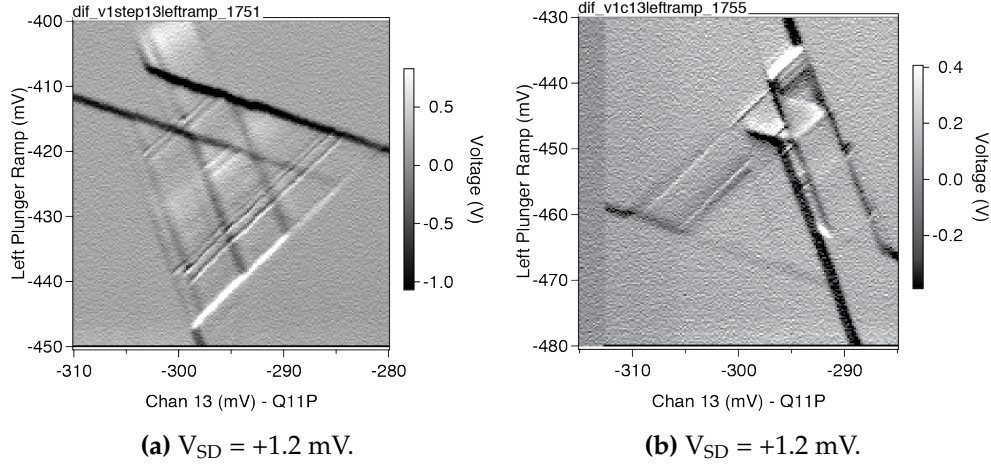


Figure 6.8: Fast reflectometry readout of S4 SQD in NO7a, sensing an electron transition in the few-electron regime for positive and negative source/drain bias. Perpendicular magnetic field: 1 T. In-plane magnetic field: 100 mT.

The transition lines correspond to the rate-limiting tunnel barriers. In this particular instance the double quantum dot was tuned to be balanced at positive source-/drain bias, revealing characteristic lines corresponding to electron tunneling between different excited states. At negative bias the structure changes dramatically, likely due to capacitive coupling of the source-side 2DEG to the quantum dots, perturbing the electronic states and tunnel couplings between dots.

It is in theory possible to decipher the internal energy levels of the quantum dots given these transitions lines, however this has not been prioritized due to the electronic environment being highly specific to the gate voltages and even source-drain bias, so at best one would learn about a very specific double dot configuration hardly translating into general knowledge.

7

Summary and outlook

During the work on this Master's project several lateral gate-defined quantum dot devices have been investigated. The CB7 sample fabricated by Christian Barthel has been used to verify the capability of our experimental setup for measurements on double quantum dots.

The NO7a device consisting of a linear array of quantum dots, measured via charge sensors, has been tuned and shown to be able to host multiple double as well as triple quantum dot systems. However, the linear design of the device did not lend itself to forming reliable asymmetric double dots, as the larger quantum dot is likely to break apart as the confining gates are tuned to negative voltages required for reaching the few-electron regime. It is possible that with additional time and device tuning an asymmetric double quantum dot can be configured in which a singlet-triplet qubit can be operated, however it has been observed to be contrary to the natural inclinations of the device, and probably one's time is better spent fabricating a device with built-in quantum dot asymmetry designed specifically for the purpose.

A reflectometry circuit was implemented, enabling fast readout of the state of a charge sensor on the device on microsecond timescales. However, the use of an SR560 Low-Noise preamplifier was found to significantly limit the measurement bandwidth. And a much higher bandwidth and correspondingly lower measurement time is theoretically realizable, and attempting a similar experimental setup without this component is a logical next step, sacrificing some signal amplitude for potential single-shot readout of the charge state of a quantum system.

Several useful software routines for experimental control have been developed, notably: Compensation of the plunger gate of a sensor quantum dot counteracting changing gate voltages, resulting in a marked improvement of the effective range; automatic calibration of a charge sensor; automatic calibration of cross-coupling factors between gates; automatic backup and easy retrieval of gate voltage config-

urations, as well as other functions of experimental use not described in this thesis but available on the QDev wiki.

Several experimental challenges related to electrical errors in the cryostat has been overcome, due in part to failures of a DC block component in the reflectometry circuit failing at cryogenic temperatures.

In the process of the experiment, experience with and knowledge of the range of instrumentation necessary to confine and measure quantum dot systems has been accumulated. This knowledge has been used to describe the experimental setup in detail, hopefully of use to new generations of experimentalists at Center for Quantum Devices.

Appendix A

Error signature of faulty DC block

During experiments, we encountered a DC block mounted on the Rx reflectometry line between the PT2 stage and the cryoamp, which failed during cooldown but worked at room temperature. The reflection spectrum of the failed DC block is included here for future reference, should a similar problem arise with the reflectometry lines.

The DC block component was a Mini-Circuits BLK-18-S+, serial no. 15542.

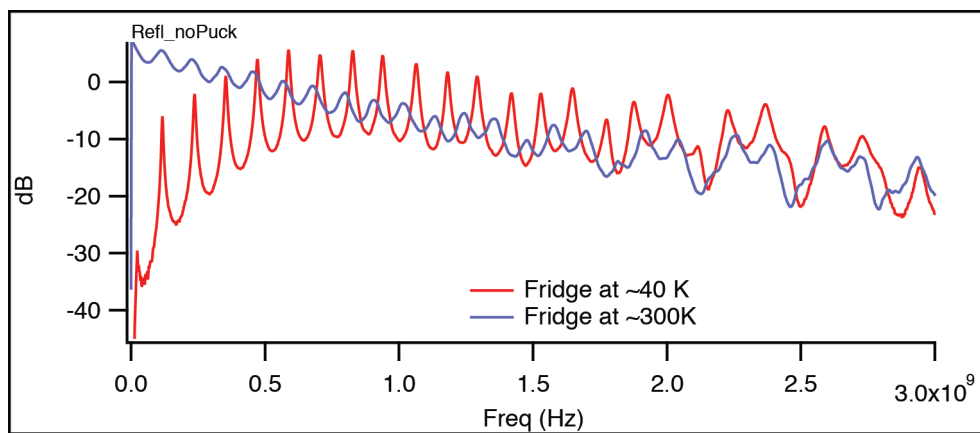


Figure A.1: S_{21} reflection from reflectometry Tx and Rx lines, measured via a HP 8753 signal analyzer. The reflections at low temperatures were caused by a faulty DC block.

Epilogue

Some time has passed now since I first strolled by the 4th floor of building D of the H.C. Ørsted institute, motivated by curiosity of the inception of the heralded fancy new laboratory for which the previous tenants of the floor had been evicted. The walls were newly painted, and I was stepping on gray paper laid to prevent dirty footprints from soiling the recent floorwork. The laboratory was populated only by some craftsmen and Charlie. He showed me around, and the topic of a Master's project came up. I had not envisioned myself as an experimental quantum physicist, but I am also not a proponent of limiting oneself to preconceived ideas about the future. The field seemed interesting as well as challenging, and Charlie struck me as a pleasant person. After some honest consideration encouraged by Charlie, I eventually applied for a position as deckhand at *SS Quantum Devices*, about to make its maiden voyage.

The new lab brought with it a cultural heritage which I have found very interesting to become acquainted with. I consider Denmark to be somewhat similar to the Shire of Tolkien's Middle Earth; as a people we are mostly content with having a pleasant time, leaving grand ambitions to the outside world, which is suspected to be mostly hypothetical to begin with. It has been an interesting challenge to adjust to another set of expectations for effort and productivity. The journey was more arduous than I have been accustomed to previously, and even if I didn't manage to climb to the heights of accomplishment I had hoped for I am proud of the goals that I did reach. I have learned many things in QDev, some of which were even related to quantum physics, although for the most part it was more of a whetstone against which I could sharpen my wits, endurance and resolve.

Yet, I have not forgotten my heritage, and while I am about to commit a *faux pas* from an American perspective I hope my modesty will be excused. At my time in university, I have found myself in the broad middle group populated by people roughly divisible in two archetypes, or perhaps linear combinations of them; people of average intelligence who worked hard, and people of above average intelligence who put in sufficient effort to meet expectations while cultivating more or less productive extra-curricular interests.

At QDev, I have found myself amongst highly intelligent people, accustomed to very hard and focused work. I suspect that it has been a very healthy place for me, and the high expectations have given me an opportunity to optimize many life habits, akin to the intellectual equivalent of anaerobic exercise. In the process I found myself exceeding the limit of the pressure which I could sustainably exert on myself, but I have no regrets; I believe that exceeding the limits is necessary to determine where they were in the first place. And with that knowledge comes the opportunity to push against them.

Inspired by some principles of RF electronics I have encountered during my time in the laboratory, I propose that the productivity of an individual can be modeled by a resonant system. Let's define the unit of productance; the value of which is determined by complex dynamics between factors such as work, rest and happiness. Optimal productance is achieved when a balance is reached, matching a resonant condition. Furthermore, each value can be optimized, changing the dynamics and enabling higher productance. Motivated by people around me, including Charlie who is perhaps the productivity equivalent of a Tesla coil, I have learned to work harder, rest hard and enjoy harder, and I have no doubt that this will benefit me wherever I will go from here in life.

It is also well-known from electronics that a high Q-factor is equivalent with a narrow bandwidth; a circuit resonating at many different frequencies will dissipate more energy per cycle. For me personally, a large part of the exercise has been to limit my bandwidth in a sense. To think less outside the box - or rather, to define a box centered around experimental physics, and training myself to stay inside it, even if it felt cramped at times. By now I have come to enjoy the box, and I can see why people would choose to stay, climbing to the very heights of the ivory tower. I don't know if that is the path for me; I have made an agreement with myself that I will try on some other boxes before I settle on one. Maybe I will never settle, roaming irreverently around the cognitive landscape. It is my impression that humanity benefits from both kinds of people.

For some, the box, whatever the nature of theirs in particular, feels like a prison. But a prison ceases to be a prison once the inhabitant learns the way out. Conversely, there are people with minds unbounded by dogma, who feel a claustrophobic repulsion to the concept of limitedness. Compulsory freedom is a prison of another form. I am convinced that some practice in changing between both perspectives is useful for all people. After all, most people agree that the most pleasant music lies somewhere on the spectrum between freeform fusion jazz and elevator music.

I would like to extend my gratitude to all the people whose company have provided help and inspiration during my time in QDev. First and foremost, Peter Dahl Nissen, who has been my primary mentor as well as colleague. Your guidance is appreciated.

Thanks to Nastasia Okulova, whose long hours in fabrication provided the basis for the actual experiments, and whose organizational efforts has been a noticeable contribution to the study environment of Nanoscience at KU.

Thanks to Ferdinand Kümme, who shared his wealth of knowledge on experimental techniques in equal amounts as his contagious joy of physics in general. His array of physics puzzles makes him the most efficient nerd sniper¹ I have yet encountered.

Thanks to Morten Kjærgaard for helpful tips on maintaining productivity as well as sanity in a high-expectation environment, as well as his pleasant company as my next-desk neighbour.

Thanks to Andrew Higginbotham, who showed me various tricks and techniques around the lab, and indirectly taught me that a simple solution started immediately nearly always gets the job done faster than an optimized solution started after careful consideration (and often, the simple solution was the optimal one to begin with).

Thanks to Sven Albrecht for stimulating discussions on diverse topics including ego and materialism. One day we'll find time to drink that coffee we've been talking about for so long.

Thanks to Katrine Rasmussen for training me in the craft of using the espresso machine in the QDev lounge, a skill that I have enjoyed honing and have benefited from continuously.

Thanks to Jess Martin for her pleasant company, her administrative work and her excellent efforts in organizing various QDev retreats and excursions. I rarely get to dine at castles otherwise.

Thanks to Katrín Hjorth for teaching me the meaning of Icelandic children's songs. Thanks also, with Jess and Tina, for filling various orders for lab equipment and keeping me well stocked with the requisition forms necessary for keeping the liquid nitrogen flowing freely. Thanks, in fact, for the company of all the people in QDev who have made my time here enjoyable.

¹See <http://xkcd.com/356/>

Finally, thanks to Charles Marcus for welcoming me aboard his vessel of experimental quantum physics; for teaching me valuable concepts such as *failing as quickly as possible* and reaching for the limits of the imaginably achievable; for adding words such as *ambit*, *lacuna*, *germane* and *epicyclical* to my English vocabulary; for delivering an excellent public lecture for *Science & Cocktails*; and generally for deeming me worthy of higher expectations than I had previously been accustomed to. I hope I didn't fail them too spectacularly.

So long QDev, and thanks for all the coffee. It has been challenging and rewarding.

- *Martin Kufahl, June 2014*

Bibliography

- [1] C. Barthel, D. J. Reilly, C. M. Marcus, M. P. Hanson, and A. C. Gossard. Rapid single-shot measurement of a singlet-triplet qubit. *Phys. Rev. Lett.*, 103:160503, Oct 2009. doi: 10.1103/PhysRevLett.103.160503. URL <http://link.aps.org/doi/10.1103/PhysRevLett.103.160503>.
- [2] C. Barthel, M. Kjærgaard, J. Medford, M. Stopa, C. M. Marcus, M. P. Hanson, and A. C. Gossard. Fast sensing of double-dot charge arrangement and spin state with a radio-frequency sensor quantum dot. *Phys. Rev. B*, 81:161308, Apr 2010. doi: 10.1103/PhysRevB.81.161308. URL <http://link.aps.org/doi/10.1103/PhysRevB.81.161308>.
- [3] C. Barthel, M. Kjærgaard, J. Medford, M. Stopa, C. M. Marcus, M. P. Hanson, and A. C. Gossard. Fast sensing of double-dot charge arrangement and spin state with a radio-frequency sensor quantum dot. *Phys. Rev. B*, 81:161308, Apr 2010. doi: 10.1103/PhysRevB.81.161308.
- [4] Christian Barthel. *Control and Fast Measurement of Spin Qubits*. PhD thesis, Harvard University, 2010.
- [5] Hendrik Bluhm. *Spin Qubits - Introduction and GaAs quantum dots*, chapter A6. 44th IFF Spring School 2013 Lecture Notes. Forschungszentrum Jülich GmbH, 2013.
- [6] Gilles Brassard, Isaac Chuang, Seth Lloyd, and Christopher Monroe. Quantum computing. *Proceedings of the National Academy of Sciences*, 95(19):11032–11033, 1998. doi: 10.1073/pnas.95.19.11032. URL <http://www.pnas.org/content/95/19/11032.short>.
- [7] Christo Buizert, Frank H. L. Koppens, Michel Pioro-Ladrière, Hans-Peter Tranitz, Ivo T. Vink, Seigo Tarucha, Werner Wegscheider, and Lieven M. K. Vandersypen. In situ. *Phys. Rev. Lett.*, 101:226603, Nov 2008. doi: 10.1103/PhysRevLett.101.226603.

- [8] Asbjørn Drachmann, Asbjørn Rasmussen, and Bjarke R. Nicolaisen. Design and measurement of IQ-RF-reflectometry circuit with low rise time. Technical report, Niels Bohr Institutet, June 2013.
- [9] J. M. Elzerman, R. Hanson, J. S. Greidanus, L. H. Willems van Beveren, S. De Franceschi, L. M. K. Vandersypen, S. Tarucha, and L. P. Kouwenhoven. Few-electron quantum dot circuit with integrated charge read out. *Phys. Rev. B*, 67:161308, Apr 2003. doi: 10.1103/PhysRevB.67.161308.
- [10] G. Feher and E. A. Gere. Electron spin resonance experiments on donors in silicon. ii. electron spin relaxation effects. *Phys. Rev.*, 114:1245–1256, Jun 1959. doi: 10.1103/PhysRev.114.1245.
- [11] R. Hanson, L. P. Kouwenhoven, J. R. Petta, S. Tarucha, and L. M. K. Vandersypen. Spins in few-electron quantum dots. *Rev. Mod. Phys.*, 79:1217–1265, Oct 2007. doi: 10.1103/RevModPhys.79.1217. URL <http://link.aps.org/doi/10.1103/RevModPhys.79.1217>.
- [12] A. P. Higginbotham, F. Kuemmeth, M. P. Hanson, A. C. Gossard, and C. M. Marcus. Coherent operations and screening in multielectron spin qubits. *Phys. Rev. Lett.*, 112:026801, Jan 2014. doi: 10.1103/PhysRevLett.112.026801.
- [13] Thomas Ihn. *Semiconductor Nanostructures: Quantum States and Electronic Transport*. Oxford Univ. Press, 2010. ISBN 9780199534425. doi: 10.1093/acprof:oso/9780199534425.001.0001.
- [14] Alexander Comstock Johnson. *Charge Sensing and Spin Dynamics in GaAs Quantum Dots*. PhD thesis, Harvard University, 2005.
- [15] Jeremy Levy. Universal quantum computation with spin-1/2 pairs and heisenberg exchange. *Phys. Rev. Lett.*, 89:147902, Sep 2002. doi: 10.1103/PhysRevLett.89.147902. URL <http://link.aps.org/doi/10.1103/PhysRevLett.89.147902>.
- [16] Daniel Loss and David P. DiVincenzo. Quantum computation with quantum dots. *Phys. Rev. A*, 57:120–126, Jan 1998. doi: 10.1103/PhysRevA.57.120.
- [17] Microwaves101. Directional couplers. <http://www.microwaves101.com/encyclopedia/directionalcouplers.cfm>.
- [18] *Triton 200/400 Cryofree dilution refrigerator manual*. Oxford Instruments, issue 3.0 edition, 2012.

-
- [19] J. R. Petta, A. C. Johnson, J. M. Taylor, E. A. Laird, A. Yacoby, M. D. Lukin, C. M. Marcus, M. P. Hanson, and A. C. Gossard. Coherent manipulation of coupled electron spins in semiconductor quantum dots. *Science*, 309(5744):2180–2184, 2005. doi: 10.1126/science.1116955. URL <http://www.sciencemag.org/content/309/5744/2180.abstract>.
- [20] Frank Pobell. *Matter and Methods at Low Temperatures*. Springer, third edition, 2007.
- [21] David M. Pozar. *Microwave Engineering*. Wiley, third edition, 2005.
- [22] D. J. Reilly, C. M. Marcus, M. P. Hanson, and A. C. Gossard. Fast single-charge sensing with a rf quantum point contact. *Applied Physics Letters*, 91(16):162101, 2007. doi: <http://dx.doi.org/10.1063/1.2794995>.
- [23] Horst L. Störmer Robert B. Laughlin and Daniel C. Tsui. The Nobel Prize in Physics 1998. http://www.nobelprize.org/nobel_prizes/physics/laureates/1998/.
- [24] R. J. Schoelkopf, P. Wahlgren, A. A. Kozhevnikov, P. Delsing, and D. E. Prober. The radio-frequency single-electron transistor (RF-SET): A fast and ultrasensitive electrometer. *Science*, 280(5367):1238–1242, 1998. doi: 10.1126/science.280.5367.1238.
- [25] D. Sprinzak, Yang Ji, M. Heiblum, D. Mahalu, and Hadas Shtrikman. Charge distribution in a kondo-correlated quantum dot. *Phys. Rev. Lett.*, 88:176805, Apr 2002. doi: 10.1103/PhysRevLett.88.176805.
- [26] *DSP Lock-In Amplifier model SR830*. Stanford Research Systems, revision 1.5 edition, 1999.
- [27] Sun Tzu. *The Art of War*. The Seven Military Classics, pre 400 B.C.
- [28] Kurt Uhlig. ³He/⁴He dilution refrigerator with pulse-tube refrigerator precooling. *Cryogenics*, 42(2):73 – 77, 2002. ISSN 0011-2275. doi: [http://dx.doi.org/10.1016/S0011-2275\(02\)00002-4](http://dx.doi.org/10.1016/S0011-2275(02)00002-4).
- [29] Klaus von Klitzing. The Nobel Prize in Physics 1985. http://www.nobelprize.org/nobel_prizes/physics/laureates/1985/.
- [30] A.T.A.M. Waele. Basic operation of cryocoolers and related thermal machines. *Journal of Low Temperature Physics*, 164(5-6):179–236, 2011. ISSN 0022-2291. doi: 10.1007/s10909-011-0373-x. URL <http://dx.doi.org/10.1007/s10909-011-0373-x>.

- [31] Herbert Kroemer Zhores I. Alferov and Jack S. Kilby. The Nobel Prize in Physics 2000. http://www.nobelprize.org/nobel_prizes/physics/laureates/2000/.